

Rivers, reefs, and deltas; Geomorphological evolution of the Jurassic of the Farsund Basin, offshore southern Norway

Thomas B. Phillips*, Christopher A-L. Jackson, Rebecca E. Bell, Ayunda A. Valencia

Basins Research Group (BRG), Department of Earth Science and Engineering, Imperial

College, South Kensington Campus, Prince Consort Road, London, SW7 2BP, UK

*Corresponding author: tbphil13@gmail.com

Abstract

Reconstructing ancient depositional environments and sedimentary facies distributions is vital to understanding the development of petroleum systems, as well as offering insights into the wider evolution of a region. However, in many underexplored, ‘frontier’ basins the identification of sedimentary facies is only possible at sparsely located wells, which are only able to document different facies in one-dimension. This is especially problematic in petroleum-bearing basins, where we typically need to define the three-dimensional distribution and geometry of source, reservoir, and seal rocks to define a working petroleum system. However, 3D seismic reflection data are able to provide detailed imaging of the earth’s subsurface across multiple stratigraphic levels. Interrogation of these data through the analysis of seismic attributes offers the opportunity to map the geometry and distribution of different facies in three dimensions. In this study, we examine the Farsund Basin, an underexplored basin located offshore southern Norway. Despite it lying in the prolific and much-explored North Sea basin, only one well has been drilled in the basin, meaning we have a very poor understanding of its hydrocarbon resource potential. Furthermore, this E-trending basin is anomalous to the N-trending basins present regionally, having experienced a different tectonic evolution, meaning that regional depositional models may not be applicable.

We undertake a seismic attribute-driven interpretation of 3D seismic reflection data to constrain the geomorphological evolution of the Farsund Basin throughout the Jurassic, thereby assessing its petroleum potential and offering broader insights into the regional tectono-stratigraphic evolution of the area. We identify a series of west-trending rivers in the Lower Jurassic, the distribution of which are controlled by syn-depositional, salt-detached faults, rather than the basement-involved faults. Subsequently, following Middle Jurassic

flooding, a series of carbonate reefs, expressed as sub-circular amplitude anomalies, developed. We identify two distinct reef morphologies, which we infer represent growth in differing water depths controlled by differential compaction of sub-reef strata across underlying, inactive faults. Within the Upper Jurassic we identify numerous curvilinear features, which are arranged into discordant sets and correspond to the downdip termination of southwards-prograding deltaic clinoforms. These deltas were deposited prior to the onset of fault activity. This study highlights how seismic attribute-driven, seismic geomorphological analysis can be used to identify facies distributions and types in areas lacking well penetrations. Furthermore, the geomorphological development of such basins, inferred directly from seismic reflection data, can be related to and help constrain their hydrocarbon potential and tectono-stratigraphic evolution.

1 Introduction

Direct information on subsurface stratigraphy and sedimentary facies is only available from boreholes, which are able to provide 1D insights into the sedimentary facies present at depth (e.g. Goldsmith et al. 1995; Michelsen et al. 2003; Holgate et al. 2013; Jarsve et al. 2014; Mannie et al. 2014). Even so, information from boreholes is often limited by relatively sparse spatial coverage and poor core recovery. Even in areas containing abundant well penetrations the ability to determine detailed 3D facies architecture, distribution and associations is still constrained by well-spacing (e.g. Johannessen & Andsbjerg 1993; Dreyer et al. 2005; Holgate et al. 2013; Mannie et al. 2014). Outcrop analogs can provide more detailed insights into the typical geometries and associations of different facies (e.g. Prélat et al. 2009; Romans et al. 2011; Agirrezabala et al. 2013; Holgate et al. 2014; Legler et al. 2014), but are unable to offer any information on the in-situ distribution and geometry of specific subsurface units.

Seismic reflection data allows us to examine the stratigraphic evolution of the subsurface, and map different facies distributions, over a greater areal extent than borehole data. Using 3D seismic reflection data, we are able to produce relatively high-resolution images (10's m) of the earth's subsurface and map the 3D geometry of ancient geomorphic landscapes across different stratigraphic levels. The evolution of these landscapes throughout geological time allows us to assess the tectono-stratigraphic evolution of an area, particularly in frontier sedimentary basins where boreholes may be lacking (e.g. Cartwright & Huuse 2005; Colpaert et al. 2007; Jackson et al. 2010; Jackson & Lewis 2013; Klausen et al. 2016; Saqab & Bourget 2016). Amplitude and frequency derived seismic attributes, such as root mean square (RMS) amplitude, variance, dominant frequency, and spectral decomposition are able to offer further information above that provided by the seismic reflection character

alone, allowing us to constrain the geomorphological evolution and 3D facies distribution of an area across geologic time (e.g. Ryseth et al. 1998; Colpaert et al. 2007; Chopra & Marfurt 2008; Jackson et al. 2010; Zhuo et al. 2014; Klausen et al. 2016; Eide et al. 2017). We conduct a seismic attribute-driven interpretation of 2D and 3D seismic reflection data located offshore southern Norway, and analyse the 3D facies architecture of the Triassic and Jurassic section preserved in the relatively underexplored Farsund Basin (Figure 1).

Data from well 11/5-1, located along the southern margin of the Farsund Basin, provides independent constraints on the lithology of the depositional elements imaged within the 3D seismic volume (Figure 1). Current paleo-geographical models within this area are largely based on regional borehole-correlation studies, with data primarily from the adjacent Egersund and Norwegian-Danish Basins and little within the Farsund Basin; these studies document a clastic-dominated net-transgressive setting throughout the Jurassic (Figure 1) (Sørensen et al. 1992; Mannie et al. 2014; Mannie et al. 2016). However, the Farsund Basin experienced a different tectonic evolution to adjacent basins, being heavily influenced by activity along the underlying lithosphere-scale Tornquist zone (Phillips et al. 2018), thus the basin likely also experienced a relatively unique stratigraphic evolution within the region and may host bespoke petroleum systems. Through detailed seismic geomorphological analysis and seismic attribute driven interpretation, we show that the Farsund Basin contains markedly different facies types and associations to adjacent basins, implying a different tectono-stratigraphic evolution. We thus provide insights into the tectonics, sedimentation history, and hinterland character of the area throughout the Jurassic, suggest reasons as to why it differs from areas nearby and help to characterise any potential petroleum systems.

Through examining the stratigraphic architecture and structural style of the Triassic interval, we determine the initial depositional limit of the Zechstein salt, trending E-W across the southern margin of the basin. Using seismic-attribute driven interpretation, we identify a

series of E-trending fluvial systems situated above the Base Jurassic Unconformity (BJU) within the Middle Jurassic. These are overlain by a series of carbonate patch reefs, expressed as sub-circular high amplitude anomalies within the seismic data, the morphology of which is reflective of the water depth in which they grew. Following a period of shale deposition in the Middle-to-Late Jurassic, a series of deltaic fans prograded across the basin. The deltaic fans were imaged in the 3D seismic volume as sets of discordant curvi-linear lineations, corresponding to downlap terminations within clinoform sequences. The geomorphological evolution of this area offers insights into the regional tectonics at the time, whilst the identified paralic-to-marine geomorphological features represent a series of potential clastic and carbonate reservoirs, which may form part of viable petroleum systems.

2 Regional geological setting

This study focusses on the E-trending Farsund Basin, located offshore South Norway (Figure 1). To the north and south the basin is bordered by the Permian-Carboniferous aged Varnes Graben and Norwegian-Danish Basin respectively (Figure 1) (Heeremans & Faleide 2004; Heeremans et al. 2004), and to the east by the much-explored Permian-Carboniferous Egersund Basin. The structural (e.g. Mogensen & Jensen 1994; Sørensen & Tangen 1995; Jackson et al. 2013; Jackson & Lewis 2013; Tvedt et al. 2013) and stratigraphic evolution (e.g. Sørensen et al. 1992; Mannie et al. 2014; Mannie et al. 2016) of the Egersund Basin has been studied by numerous authors. It is separated from the Farsund Basin by the Stavanger Platform and Lista Nose fault blocks (Hamar et al. 1983; Skjerven et al. 1983; Jackson & Lewis 2013; Lewis et al. 2013) (Figure 1). To the west the Farsund Basin opens into the Norwegian-Danish Basin and Sorgenfrei-Tornquist fault complex (Figure 1) (Nielsen 2003; Heeremans et al. 2004; Olivarius & Nielsen 2016).

The southern margin of the Farsund Basin is defined by the N-dipping Fjerritslev Fault system (Figure 1), which within the 3D seismic volume comprises the Fjerritslev North and Fjerritslev South Faults to the north and south respectively (Figure 2a). A further E-W striking fault, termed the Farsund North Fault and located outside of the 3D volume, forms the northern margin to the basin (Figure 1). A series of N-S-striking faults are present across the southern margin of the basin (Figure 2a); the two largest of which control the preservation of Triassic strata and are termed NS1 and NS2 from north to south respectively (Figure 2a). At shallower stratigraphic levels, N-S striking faults are largely absent; with the basin morphology dominated by the E-W Fjerritslev North and South faults (Figure 2b, c). A detailed analysis of the structural evolution of the Farsund Basin can be found in Phillips et al. (2018).

The Farsund Basin is situated along the northern margin of the North Permian Basin, which contains mobile evaporites of the Upper Permian Zechstein Supergroup (Christensen & Korstgård 1994; Heeremans et al. 2004; Jackson & Lewis 2013). The Triassic was associated with activity along N-S striking faults, such as NS1 and NS2 (Figure 2c), and the deposition of a non-marine sedimentary succession (McKie & Williams 2009; Jarsve et al. 2014). Widespread uplift and erosion occurred across large parts of the Central North Sea during the Middle Jurassic in response to uplift of the Mid-North Sea thermal dome located to the west (Rathey & Hayward 1993; Underhill & Partington 1993), resulting in the erosion of Triassic-to-Lower-Middle Jurassic strata and the formation of the BJU across the Farsund Basin (Figure 3). Structurally, the Middle-Late Jurassic represents a period of relative tectonic quiescence within the Farsund Basin (Phillips et al. 2018). A regional rift phase is documented across the North Sea from the Late Jurassic-to-Early Cretaceous (Ziegler 1992; Færseth 1996; Coward et al. 2003), which led to the formation of the E-W striking faults, i.e. the Fjerritslev North and South faults and the Farsund North Fault that define the present-day

morphology of the Farsund Basin (Figure 1, 2a) (Mogensen & Jensen 1994; Sørensen & Tangen 1995; Phillips et al. 2018).

3 Dataset and methodology

Seismic interpretation was primarily undertaken on a 500 km² 3D seismic reflection dataset located across the southern margin of the Farsund Basin (Figure 1). These data image to 4 seconds two-way-time (TWT) (c. 6 km) with inline and crossline spacings of 18.75 and 12.5 m respectively. Frequency throughout the data ranges from 25-40 Hz, with a mean frequency in the interval of interest (0.75-1.3 s) of ~35 Hz (Figure 4). Based on this frequency, and using a velocity of 2.5 kms⁻¹ for the overlying sedimentary cover (based on well 11/5-1), we determine a vertical resolution of c. 18 m. Similarly, the limit of detectability in the data ($\lambda/30$) is ~2 m (Slatt 2006).

We carried out additional seismic interpretation on a series of N-S oriented 2D seismic sections (Figure 1), which image to 7 s TWT (c. 15 km) and allow interpretation of the stratigraphic horizons over a wider area, providing a more regional perspective to our interpretations. Seismic data are displayed as zero phase; the 3D seismic volume follows the SEG normal polarity convention; that is, a downward increase in acoustic impedance is represented by a peak (black), and a downward decrease in acoustic impedance is represented by a trough (red) (Figure 3), the 2D seismic data follow the reverse polarity convention. The ages of key stratigraphic horizons are constrained through wells 11/5-1, 10/7-1, 10/8-1, 10-5/1, 11/9-1 and 11/10-1 (Figure 1). Well 11/5-1, the only well located within the 3D seismic volume (Figure 2), provides detailed 1D facies information within the study area and is tied to the seismic interpretations through a seismic-well tie (Figure 5). Seismic attributes, such as RMS amplitude, variance, dominant frequency, and spectral decomposition were calculated within windows located either above, below or between specific key horizons in order to further interrogate and extract information from the seismic data (see Appendix A for details regarding specific seismic attributes).

We used GeoTeric software in order to calculate the spectral decomposition attribute. To do this, we extracted a frequency spectrum from the data and split this into a series of discrete bins, each corresponding to a range of 10 Hz (Figure 4). Frequency values centred on 22, 30 and 45 Hz were assigned to the colours Red, Green and Blue respectively and blended to produce the spectral decomposition attribute (Figure 4).

4 Regional stratigraphy

In this section we detail the directly sampled stratigraphic succession penetrated in numerous wells regionally, paying particular attention to well 11/5-1 located within the 3D volume (Figure 2, 5).

No Triassic strata are encountered in well 11/5-1, with Jurassic strata unconformably overlying the Upper Permian Rotliegend Group due to erosion by the BJU (Figure 3, 5). Middle Jurassic (Bajocian-Bathonian) strata of the Bryne Formation directly overlie Upper Permian Rotliegend Group strata, with Lower Jurassic rocks absent. Although not penetrated in well 11/5-1 (Figure 5), the Bryne Formation in the adjacent Egersund Basin comprises non-marine sandstone and siltstone (Vollset & Doré 1984; Mannie et al. 2016). At stratigraphically higher levels, and resting unconformably atop the BJU within well 11/5-1, is the Mid-Jurassic (Callovian) Sandnes Formation, comprised of 45 m of predominantly marine sandstone and mudstone, with some carbonate-dominated areas (containing abundant m-scale carbonate stringers) identified in well 11/5-1 (Figure 5) (Vollset & Doré 1984; Mannie et al. 2016). The Late Callovian-to-Early Volgian Egersund and Tau formations overlie the Sandnes Formation. These make up the majority of the Jurassic interval within the Farsund Basin (189 m) and, within well 11/5-1, consist of organic-rich claystones and shales (Figure 5). Isolated glauconitic and pyritic layers are present throughout these units,

indicating a low-energy, anoxic depositional environment (Figure 5) (Vollset & Doré 1984).

The uppermost Jurassic to lower Cretaceous interval consists regionally of marine shales corresponding to the Sauda Formation; however in well 11/5-1, the upper 15 m of the 22m thick Sauda Formation (incorporating the lowermost Lower Cretaceous interval) is sandstone-dominated (Figure 5). The Jurassic interval is overlain by a large thickness of Lower Cretaceous deepwater claystones and mudstones.

5 Seismic geomorphological observations and interpretation

Well 11/5-1 provides direct constraints, albeit only in one dimension, on the stratigraphy of the Triassic and Jurassic succession of the Farsund Basin. Now, we use a suite of seismic attributes (see Appendix A) to determine the 3D geometry and distribution of facies within the basin, linking to those directly sampled by the well, and comparing to facies types and distributions observed regionally. In each subsection, we first describe our seismic geomorphological observations, based on seismic reflection, seismic attribute and well data analysis before posing an interpretation for the likely depositional environment and geomorphological origin of the identified features.

5.1 Triassic – Limit of thin-skinned tectonics and depositional extent of mobile Zechstein salt

In the North Permian Basin, Zechstein salt is overlain by Triassic strata (Clark et al. 1998; Lewis et al. 2013). Post-depositional salt mobilisation and modification means that the initial depositional limit of salt and salt basins is often uncertain (Clark et al. 1998; Jackson & Lewis 2013). Triassic strata in the Farsund Basin are dominated by S-dipping, salt-detached normal faults, related to southwards directed salt-mobilisation into the Norwegian-Danish Basin (Figure 6). The top of the Triassic interval is eroded by the BJU, with Triassic strata largely absent across the footwalls of NS1 and NS2, north of the Fjerritslev South Fault (Figure 3, 5). The Fjerritslev North and South faults in this area do not show any pre-Cretaceous activity and were not present during the Triassic, with the Fjerritslev South Fault appearing restorable up to the BJU (Figure 3, 6) (Phillips et al. 2018).

Within the hanging wall of the Fjerritslev South Fault, a series of small-scale (c. 50 ms TWT, 70 m height) clinoforms are identified in the Triassic interval, prograding towards the south; forming a marker horizon within the interval (Figure 6). The relatively small height

of these clinoforms implies deposition within a shallow, fluvio-deltaic shoreface environment (cf. Patruno et al. 2015a). Immediately south of these clinoforms, now located on the footwall of the Fjerritslev South Fault, thin-skinned salt-detached faulting is restricted northwards (Figure 6). We propose that this transition from the preserved clinoform sequence in the north, to where they are bisected by numerous thin-skinned salt-related faults in the south, marks the initial depositional limit of the mobile component of the Zechstein salt (Figure 6). North of this limit, mobile Zechstein salt is not present, although thin salt or a less mobile facies, both unable to flow, may be present. We propose the following model; prior to salt mobilisation, deltaic clinoform sequences prograded southwards across the location of the present-day Fjerritslev South Fault and over the Zechstein salt basin (Figure 6). Following the onset of salt mobilisation during the Triassic, areas with underlying Zechstein salt were subject to the formation of thin-skinned salt-detached faults, whereas areas north of the initial depositional limit, containing no underlying salt, were unaffected, as demonstrated by the preserved clinoform sequences (Figure 6). Using these criteria we are able to map the original depositional limit of mobile Zechstein salt trending E-W across the footwall of the Fjerritslev South Fault (Figure 1). To the east, the depositional limit of the Zechstein salt takes an abrupt step northwards across NS2, before continuing in an E-W orientation across the Farsund Basin (Figure 1).

5.2 Bryne Formation – Fluvial systems

A series of high-amplitude reflections, which are not sampled by well 11/5-1 (Figure 3), are observed atop the BJU along the footwall of the Fjerritslev South Fault (Figure 7). Due to the restricted lateral extent of these reflections, and their stratigraphic position below the Sandnes Formation, we interpret that these reflections correspond to the Bryne Formation and thus represent the oldest Jurassic strata in the Farsund Basin. We identify two discrete, laterally discontinuous high-amplitude tuned reflections, implying thicknesses less than the

vertical resolution of the data (c. 20 m), that are each around 500 m wide (Figure 7). The high-amplitude bodies largely appear to be situated in the hanging wall of thin-skinned, salt-detached faults, with few faults present directly beneath the bodies themselves (Figure 7).

We extract RMS amplitude, variance and dominant frequency seismic attributes, calculated within a 25 ms TWT window above the top of the BJU horizon in order to encompass the full thickness of the features, to highlight the 3D geometry of these high-amplitude bodies and provide clues as to their geological origin (Figure 7). In map view, the RMS amplitude attribute highlights two E-W trending high-amplitude features, with curvilinear channel-like geometries, on the footwall of NS2, termed Channel 1 and Channel 2 from north to south respectively (Figure 8). Channel 1 is c. 8 km long and terminates to the west in the footwall of the Fjerritslev South Fault. This channel is not imaged in the hanging wall of the Fjerritslev South Fault, due to the amplitude signal being masked by higher background amplitudes (Figure 8). Channel 2 originates within the footwall of the Fjerritslev South Fault, has an overall length of c. 9 km, and widens eastwards from c. 200 m to c. 400 m (Figure 8). In cross-section the channels display an asymmetric geometry, with Channel 2 being thicker towards the south (Figure 7). Both channels cross-cut and are seemingly unaffected by NS2 to the east (Figure 8). Crossing NS2, the channels widen from c. 500 m in the footwall, to c. 2 km in the hanging wall. Furthermore, the channels display a more SE orientation within the footwall of the fault (Figure 8).

The variance and dominant frequency seismic attributes provide more detailed insights into the channel geometry. The variance attribute highlights a series of minor linear channels oriented perpendicular to, and joining along both channel 1 and 2. These secondary channels display typical lengths and widths of 400 m and 150 m respectively (Figure 8c). In some instances these minor channels link Channel 1 and Channel 2 (Linking channel on Figure 8e). The secondary channels display an asymmetric distribution with respect to the

main channel, being concentrated along one margin which displays a relatively shallow gradient. The opposite margin of the channel is more sharply defined and is often associated with an underlying salt-detached fault (Figure 7, 8). The dominant frequency attribute further defines the first-order geometry of the channels within the footwall of NS2, which are delineated by relatively high frequencies. Frequency decreases along the channel, from c. 45 Hz in the west, to c. 35 Hz in the east, potentially indicating a thickening along the channel interval from west to east (Figure 8d).

Based on the seismic attribute-derived observations described above, we interpret these channel-like features as originally E-flowing, Middle Jurassic fluvial systems, now preserved within the Bryne Formation. The high-amplitude character of the channels indicates a different, perhaps more sand-prone, lithology to the Egersund and Sandnes formation mudstone above and potentially fine-grained lithologies below (Figure 5, 7). We interpret the smaller structures merging along the margins of the main channels as tributaries (Figure 8e). True thicknesses are difficult to ascribe to these channels due to their tuned seismic reflection response (Brown 2011). The vertical resolution of the data ($\lambda/4$; 20 m), represents a maximum thickness estimate for the channels. The E-W orientation of these channels is partly controlled by underlying thin-skinned, salt-detached faults. In some instances, these underlying faults appear associated with a more sharply-defined channel margin, indicating that activity on these faults influenced the paleo-free surface (Figure 7, 8). The adjacent margin is associated with a gentler gradient and hosts numerous tributaries (Figure 8e). Towards the west the channels widen across the thick-skinned NS2 fault (Figure 8), potentially transitioning from a fluvial to a more deltaic or restricted lacustrine environment. Based on this, we propose that NS2 represents the paleo-shoreline during the deposition of the Bryne Formation.

5.3 Sandnes Formation – Patch reef development

Atop the Bryne Formation channel systems, a series of isolated high-amplitude features (IHAFs) are identified within a stratigraphic interval corresponding to the Middle Jurassic Sandnes Formation, which overlies the BJU and, where present, the Bryne Formation. As penetrated in well 11/5-1, the Sandnes Formation consists of sandstone and mudstone, with some isolated carbonate stringers also present. No IHAFs are directly penetrated by the borehole (Figure 5).

In cross-section, the IHAFs display a double (peak-trough) reflection character, with a large positive impedance contrast at the top (Figure 9). Two distinct IHAF morphologies are identified; short, wide structures with heights of 25 ms TWT (c. 30 m), and taller, narrower structures with typical heights of 35 ms TWT (c. 50 m) (Figure 9). The plan-view morphology of the IHAFs is further highlighted by seismic attributes (Figure 10). RMS amplitude, variance and dominant frequency attributes were extracted from a 50 ms window above the BJU and also above the Bryne Formation channels, ensuring coverage of the full height of the structures and a lack of input from stratigraphically lower features. In map-view the IHAFs are expressed as circular to sub-circular high amplitude anomalies, consisting of a high amplitude core and relatively low amplitude margin (Figure 10). A total of 333 IHAFs are identified across the area; smaller IHAFs are most accurately delineated using the spectral decomposition attribute (Figure 10c). The larger structures have a diameter of c. 450 m; whilst the smaller structures have a diameter of c. 150 m (Figure 9, 10). The tall, narrow IHAFs are predominately situated within the hangingwall of NS2, whereas the short, wide IHAFs are restricted to the footwall (Figure 10d). Notably, the distributions of the two different morphologies are unaffected by the E-trending Fjerritslev North and Fjerritslev South faults that dominate the present-day basin morphology, with the wider, shorter IHAFs situated on both the hangingwalls and footwalls of the Fjerritslev North and South faults

(Figure 10). The distribution of the IHAFs does not change laterally to the south and west, indicating that the IHAF domain may extend outside of the 3D volume. However, the concentration of the IHAFs does decrease to the NE, in the hanging wall of both NS2 and the Fjerritslev North Fault, implying that this may represent the limit to the IHAF domain (Figure 10).

In some instances the IHAFs are cross-cut by later faults (Figure 10d, f), implying that they are brittle in nature. Some IHAFs display non-rounded, more elongate geometries, which RMS amplitude shows is typically a result of these IHAFs containing multiple high amplitude nuclei. The typical sub-rounded morphology of the IHAFs implies a radial mode of growth, with those IHAFs that contain multiple nuclei representing IHAFs that have grown radially and since merged (Figure 10e).

A variety of different processes can lead to the formation of sub-circular structures in seismic reflection data (Stewart 1999), including volcanic edifices (both igneous and mud-related) (Davies & Stewart 2005), hydrothermal vent systems (Magee et al. 2016), gas accumulations and pockmarks (Hovland et al. 1987; Fichler et al. 2005; Andresen et al. 2011; Agirrezabala et al. 2013; Marcon et al. 2013), carbonate reefs (Posamentier & Laurin 2005; Rosleff-Soerensen et al. 2012; Saqab & Bourget 2016) and evaporite structures (Jackson & Talbot 1986). Based on the relatively small (100's m scale) scale of the structures, coupled with a lack of igneous activity within this area at this time, we discount an igneous/volcanic edifice related origin for the IHAFs. Similarly, the small-scale of the IHAFs, and the lack of regional igneous activity also discounts an origin as hydrothermal vent systems (Magee et al. 2016). In addition, we do not consider an evaporate-related origin based on the IHAFs being located stratigraphically above the Upper Permian Zechstein salt, and there being no Jurassic salt present in this area of the North Sea (Jackson & Lewis 2013). Furthermore, the IHAFs are also present north of the aforementioned depositional limit of the Zechstein salt (Figure 1,

6). The relatively small-scale nature of the structures would be consistent with an origin as pockmarks; however, the structures are associated with positive relief whereas pockmarks would typically form cavities infilled with material from overlying strata (Hovland et al. 1987; Agirrezabala et al. 2013; Kluesner et al. 2013; Marcon et al. 2013).

Therefore, based on: i) their radial growth mode; ii) the positive impedance contrast at the top of the structures; iii) their overall size and morphology, along with the binary nature of the size distribution potentially reflecting different growth conditions; and iv) their brittle nature, we interpret that the IHAFs represent a series of carbonate patch reefs. Carbonate is present locally, as demonstrated by the carbonate-rich intervals penetrated in well 11/5-1 (Figure 5). Modern-day carbonate patch reefs are typically found within shallow marine environments and are often associated with sheltered lagoonal areas. Modern patch reefs have diameters of c. 200 m, and heights of c. 10 m, similar to those within the study area (e.g. Brock et al. 2008; Purkis et al. 2015). In addition, carbonate patch reefs have previously been identified on seismic reflection data, displaying similar geometries, morphologies and seismic character to the IHAFs identified here (Posamentier & Laurin 2005; Ruf et al. 2008; Rosleff-Soerensen et al. 2012; Saqab & Bourget 2016). No larger-scale atolls or barrier reefs are identified in the Farsund Basin, unlike in other examples (Rosleff-Soerensen et al. 2012; Saqab & Bourget 2016), although it may be that a barrier reef is simply situated outside of the 3D seismic volume. Alternatively, the reefs within the Farsund Basin may be located in a natural sheltered environment.

5.4 Egersund and Tau formations – Deposition of anoxic shales

The patch reef-hosting Sandnes Formation is overlain by the Upper Jurassic Egersund and Tau formations (Figure 3, 5). As determined from boreholes regionally, including well 11/5-1 in the Farsund Basin, these formations typically comprise organic-rich shales (Figure

5). Within the Farsund Basin, the Tau Formation has a slightly elevated Gamma Ray value (c. 120 API) when compared to the underlying Egersund Formation (c. 110 API) (Figure 5). Both formations are associated with a poorly reflective seismic facies within the basin (Figure 3, 5). Based on the observations outlined above, we interpret that the deposition of both the Egersund and Tau formations occurred in a low-energy environment, with the presence of pyritic and glauconitic horizons suggesting periodic anoxic conditions (Figure 5). Such an environment may indicate a sea level rise and marine transgression since the deposition of the Sandnes Formation, with deposition occurring in a deep marine environment, or may alternatively indicate deposition within a restricted, more lagoonal environment.

5.5 Sauda Formation - Delta progradation

A package of high-amplitude reflections is present at the top of the Jurassic interval, corresponding to the Sauda Formation in well 11/5-1 (Figure 3, 11). This reflection package is c. 40 ms TWT (c. 50 m) thick, thinning southwards, and is associated with lateral changes in amplitude and small-scale clinoform sequences that downlap towards the south (Figure 11). These downlap terminations often correspond to the areas of amplitude brightening (Figure 11). The top and base of the high amplitude reflection package was mapped throughout the 3D volume, along with individual internal horizons; seismic attributes were extracted from between the top and base horizons (Figure 11).

RMS amplitude, spectral decomposition and dip azimuth seismic attributes highlight a series of divergent, curvi-linear lineations in plan-view, defining high- and low-amplitude packages of varying frequency (Figure 12). Each band is c. 400 m wide, diverges westwards and displays a concave-to-south planform geometry. The bands are arranged into a series of discordant sets and thus truncate each other, at either low (i.e. Sets 1-3 in Figure 12d) or high

angles (i.e. Set 4 in Figure 12d). Additional internal sets and truncations may tentatively be present, although these are not clear and accurately delineated within the data (Figure 12). The lineations are ubiquitous across the whole of the study area apart from across the footwall of the Fjerritslev South Fault, where the Sauda Formation is absent due to erosion (Figure 2, 12). The lineations are seemingly unaffected by the Fjerritslev North Fault, which cross-cuts but does not noticeably offset the lineations (Figure 12). A set of N-S striking lineations are present on the footwall of NS1 (Set 4; Figure 12), displaying a concave to the east, and diverging to the southwest geometry. These N-S striking lineations also appear unaffected by the Fjerritslev North Fault, although their location, along the footwall of the N-S striking NS1, indicate that they may be influenced by this fault (Figure 12d). In some instances there appear to be mutual cross-cutting relationships between individual sets of lineations (i.e. Set 2 and Set 4 in Figure 12d), rather than truncations against one another. However, we suggest that these cross-cutting relationships are due to signal mixing within the attribute extraction window; i.e. closely superposed sets produce cross-cutting relationships and their relative age cannot be distinguished in plan-view (Figure 12). The prominent lineations observed in plan-view (Figure 12) appear to correspond to the downlap terminations of clinoform sequences in cross-section (Figure 11).

Discordant sets of high-amplitude lineations identified in seismic reflection data, superficially similar to those observed here, have previously been interpreted as ancient shoreface beach ridge environments (Jackson et al. 2010; Klausen et al. 2015; Klausen et al. 2016). Such beach ridge systems typically comprise sand-rich ridges separated by elongate, typically lower energy, depressions (Otvos 2000), and form cusped, concave-to-coastline morphologies comprising multiple discordant sets, formed through longshore drift transport (Billy et al. 2014; Vespremeanu-Stroe et al. 2016). However, although geometrically similar, based upon the lines of evidence outlined below we discount a beach-ridge origin for the

lineations within the Farsund Basin. Firstly, the amplitude changes associated with the upper Jurassic curvi-linear features within the Farsund Basin are located downdip, or below the small-scale clinoform sequences (Figure 11), rather than being associated with the topsets as would be expected with a beach ridge interpretation (e.g. Jackson et al. 2010; Billy et al. 2014). Instead, the observed amplitude brightening may represent the tuned seismic response of the breakpoint (Dreyer et al. 2005) or down-dip terminations of the clinoforms themselves (Eide et al. 2017). Secondly, the concave-to-south planform geometries of the lineations would suggest that the paleo-shoreline was north-facing, an interpretation largely incompatible with the regional setting of the basin during the Late Jurassic, which was open to the south (Figure 1, 12).

Finally, further to the arguments presented above, perhaps the most convincing evidence against a beach ridge origin for these lineations lies in their regional context. Using regional 2D seismic data, the high-amplitude lineations can be traced outside of the 3D volume. Here, they correspond to the lateral terminations of larger lobate high-amplitude packages (Figure 13, 14). These packages thicken northward, with each composed of multiple high-amplitude bodies that appear to downlap onto the underlying one, forming an overall aggradational sequence (Figure 13). Accordingly, the oldest unit is the furthest outboard (i.e. the furthest south), with younger reflections aggrading and downlapping onto one another (Figure 13). This aggradation may indicate a slow sea level rise throughout the deposition of this unit, followed by an increase in the rate of sea level rise at the onset of faulting within the basin and the deposition of the Early Cretaceous (Figure 13). The individual packages are also partitioned laterally, forming a series of discrete lobes, with terminal downlapping reflections and associated brightening at each side (Figure 14). Based on the downlap terminations we identify three main lobes from west to east, with the easternmost margin defined by an end in amplitude brightening (Figure 14).

The terminal downlap termination of these lobes forms an arcuate geometry in plan-view (Figure 15). Individual lobes are c. 100 ms TWT (c. 140 m) thick and reach around 20-40 km wide (Figure 14, 15); they prograde southwards, and appear to be sourced from the north. The lobes appear to continue northwards into the Varnes Graben, which may represent a sediment pathway from the mainland (Figure 13), although due to a lack of data coverage we are unable to constrain their geometry in this area. Similar to within the 3D volume, individual lobes display discordant relationships with one another as younger lobes overlap and stack atop underlying older ones (Figure 14, 15). The central lobe corresponds to the major lineations observed within the 3D volume (Set 2-3; Figure 12). This lobe is situated at shallower stratigraphic levels and appears to overlap the lobe situated to the east (Figure 15). Set 3 within the 3D volume may also represent an older, stratigraphically deeper lobe that has been overlapped by the main central lobe of sets 2 and 3 (Figure 12, 15). The central lobe appears to be overprinted by those to the west, incorporating the lineations observed along the footwall of NS1 (Set 4, Figure 12d), as the thickness of the Upper Jurassic sequence increases westwards (Figure 14). This thickness change is representative of increased aggradational lobe stacking to the north and west (Figure 13, 15). We suggest that the internal downlap terminations within individual lobes may give rise to the lineations observed in the 3D data (Figure 12). Furthermore, we suggest that overprinting and vertical aggradation of different generations of lobes may give rise to the discordant truncations of different lineation sets (Figure 12), with older lobes being partially overlapped by those stratigraphically shallower (Figure 15).

Based on this regional information, and in conjunction with the evidence outlined previously, we interpret that the lineations within the Upper Jurassic Sauda Formation correspond to the downlap termination of clinoforms within stacked deltaic lobes, which formed through the progradation and aggradation of a shelf slope margin (Sneider et al.

1995). This interpretation is based on: i) the lobate geometry of the individual sequences (Figure 14, 15); ii) lateral downlap terminations at the margins of lobes (Figure 13, 15); iii) small-scale clinoforms indicative of deposition within a relatively shallow environment (Patruno et al. 2015a; Eide et al. 2017) (Figure 11, 13); iv) regressive stacking of individual delta sequences indicating aggradation and deposition during an overall marine transgression (Figure 13); and v) progressive landward onlapping of the Sauda Formation by Lower Cretaceous strata (Figure 13, 14). The Sauda Formation overlies the Egersund and Tau formations (Figure 5), which were deposited within an anoxic environment. A corollary of the interpretation here is that these anoxic shales were likely deposited within a restricted, rather than deep-water environment, as the latter would require a drastic shallowing between the deposition of the two formations.

5.6 Summary of geomorphological evolution

Using a seismic attribute driven approach, we propose the following scenario for the geomorphological evolution of the Farsund Basin from the Triassic and throughout the Jurassic. Our evolution differs to those proposed regionally and provides insights into the structural evolution of the basin and the regional tectonic setting. Following a prevailing non-marine environment throughout the Triassic, the Farsund Basin represented a fluvial-coastal plain environment during the Early Jurassic, as evidenced by fluvial channels in the Bryne Formation (Figure 8). The Sandnes Formation represents a shallow marine environment, containing numerous carbonate patch reefs. Subsequently, the depositional environment transitioned to a lagoonal or restricted-marine setting during the deposition of the Egersund and Tau formations. Shale deposition was interrupted in this area by local progradation of the shelf margin and an input of sandy material, with offshore deltas identified in the Farsund Basin (Figure 12), comprising the Sauda Formation.

6 Discussion

Our model for the geomorphological evolution of the Farsund Basin, and our interpretations of the different facies present (Figure 16), differs drastically from those predicted by regional borehole correlation-based studies (Figure 1). Here, we first compare and contrast our model for the geomorphological evolution of the Farsund Basin outlined above to that more regionally, before discussing the implications for the structural evolution of the basin and regional tectonic activity, and the viability of petroleum systems in the area.

6.1 Regional paleo-geographical setting

The North Sea represented a predominately non-marine environment during the Permian, as recorded by deposition of the Rotliegend Group (Glennie 1997; van Wees et al. 2000; Glennie et al. 2003). Deposition of Zechstein salt in the Upper Permian occurred during a marine transgression and basin flooding (Glennie 1997; Glennie et al. 2003). East of the Farsund Basin, Jackson & Lewis (2013) define the depositional limit of mobile Zechstein salt striking ESE across the Lista Fault Blocks (Figure 1). We find that this limit continues eastwards along-strike across the southern margin of the Farsund Basin, and did not extend north as far as previously described (Heeremans et al. 2004) (Figure 1). The local occurrence of small-scale, likely fluvio-deltaic, clinoforms (Patrino et al. 2015a) (Figure 6), and the non-marine Smith Bank and Skagerrak formations regionally (e.g. Goldsmith et al. 1995; McKie & Williams 2009; Jarsve et al. 2014), indicates a return to a sub-aerial environment and a marine regression during the Triassic. The Triassic clinoforms were likely sourced from mainland Scandinavia to the north, and likely prograded southwards through the Varnes Graben (Figure 1).

Following Early-Mid Jurassic uplift, erosion and eventual deflation associated with the Mid North Sea thermal dome (Underhill & Partington 1993), the first formation to be

preserved regionally was the Middle Jurassic Bryne Formation. This formation is encountered in the Egersund Basin, Norwegian-Danish Basin and the Danish Central Graben, where it consists of stacked fluvial and floodplain deposits deposited in a coastal-plain environment (Sørensen et al. 1992; Johannessen & Andsbjerg 1993; Andsbjerg 2003; Michelsen et al. 2003; Mannie et al. 2014; Mannie et al. 2016). Within the Farsund Basin, the Bryne Formation is represented by two E-trending channels deposited within a fluvio-deltaic environment (Figure 8e). At a regional scale the E-W orientation of these channels may be influenced by the Mid Jurassic thermal dome (Underhill & Partington 1993), flowing away from the site of maximum uplift. Alternatively, and in the authors view more likely, channel orientation may be controlled by more local uplift related to the Lista Nose Fault blocks and Stavanger Platform to the west (Figure 1).

The Middle-Upper Jurassic (Callovian) Sandnes Formation documents a basinwide marine transgression, transitioning from a sub-aerial to shallow marine depositional environment, as observed elsewhere within the North Sea (Michelsen et al. 2003; Mannie et al. 2014; Mannie et al. 2016). This transgression was driven by a eustatic sea-level rise (Vail & Todd 1981; Sørensen et al. 1992), and may have been further augmented by rift-related thermal subsidence relating to a Permian-Triassic rift phase (Ziegler 1992). Within the Farsund Basin, the Sandnes Formation is manifest as a series of carbonate patch reefs (Figure 10), whereas elsewhere, including in the adjacent Egersund Basin, it contains only siliciclastic sediments (Figure 1b, 16) (e.g. Sørensen et al. 1992; Mannie et al. 2014; Mannie et al. 2016). The formation of carbonate patch reefs requires a lack of clastic sedimentation within a relatively sediment starved basin. The lack of sediment within the Farsund Basin at this time, compared to the Egersund Basin (Mannie et al. 2014; Mannie et al. 2016) may reflect differences in their respective onshore source areas, and suggests that they were not linked at this time.

In the Egersund Basin, facies shallow eastwards from offshore marine to shoreface, and onlap the Stavanger Platform (Mannie et al. 2014). A similar water depth change occurs within the Farsund Basin, with deeper water facies present in the east, as represented by establishment of taller and, we infer, deeper-water patch reefs (Figure 9, 10, 16), and a shallower water environment towards the west dominated by shorter and wider patch reefs. These complementary east- and west-facing shorefaces, and their associated distinct facies belts (i.e. carbonate in the east and siliciclastic in the west) indicate a relative high between the Egersund and Farsund Basins, potentially represented by Stavanger Platform and Lista Nose Fault Blocks (Hamar et al. 1983; Sørensen et al. 1992). One such topographic high, the Eigerøy Horst, continues northwards, as a series of bathymetric highs termed the Hidra Mountains, to the Norwegian mainland where it may reflect an onshore drainage divide (Rise et al. 2008).

Further sea-level increase is recorded by the deposition of the anoxic shales of the Egersund and Tau formations (Vollset & Doré 1984; Sørensen et al. 1992). Cessation of carbonate patch reef growth may have occurred due to a basin-wide transgression, or the added input of the anoxic shales (Figure 16). This transgression continued into the Upper Jurassic with the deposition of fine grained siltstones and claystones comprising the Sauda Formation (Vollset & Doré 1984; Mannie et al. 2014). A series of southwards-prograding and aggrading deltas are present within the Farsund Basin (Figure 15, 16). These fans are largely from an extra-basinal source, likely the Norwegian mainland following transport through the Carboniferous-Permian-aged Varnes Graben (Heeremans et al. 2004). Jarsve et al. (2014) previously proposed the Varnes Graben acts as a sediment pathway during the Triassic. Fan one however, may have a local sediment source, related to degradation of the Eigerøy Horst, which in this area forms the footwall of the Farsund North Fault (Figure 15). As with the

stratigraphically older patch reefs, these fans are also restricted westwards of, and are not present on, the Stavanger Platform (Figure 17).

West of the Stavanger Platform, additional deltaic sequences, the Hardangerfjord and Sognefjord units, are present within the Sauda Formation, sourced from and draining western Norway (Dreyer et al. 2005; Somme et al. 2013; Patruno et al. 2015b) (Figure 17). Wells penetrating the proximal part of the Hardangerfjord unit penetrate a mudstone dominated unit (Somme et al. 2013), whereas the Sognefjord unit has been shown to be more sandstone dominated (Patruno et al. 2015b). Within the Farsund Basin, well 11/5-1 penetrates a silty sandstone/sandstone interval corresponding to the distal part of the delta sequence; furthermore, the surrounding sediments are largely dominated by mudstones and siltstones (Figure 5), so a more sandstone-rich interval would produce the observed large impedance contrast (Figure 11, 13).

The partitioning between the Farsund deltaic sequence described here, and the Hardangerfjord unit located west of the Stavanger Platform appear to reflect the location of the drainage divide onshore Norway (Figure 17). Sediments sourced from west of the divide are deposited into the Hardangerfjord unit (Somme et al. 2013), and those east of the divide being deposited into the Farsund Basin and Skagerrak Sea (Somme et al. 2013; Jarsve et al. 2014) (Figure 17). The offshore continuation of this divide may be represented by the highs of the Eigerøy Horst, Stavanger Platform and Lista Nose Fault Blocks (Hamar et al. 1983; Skjerven et al. 1983) (Figure 17).

We have shown that the Farsund Basin contains different facies associations and experienced a markedly different tectono-stratigraphic evolution to basins to the west, separated by the Stavanger Platform and Lista Nose Fault Blocks. This may correspond to a boundary between different structural domains, between Caledonian Orogeny and post-

orogenic collapse-dominated tectonics to the west (Phillips et al. 2016), and an evolution dominated by the Sorgenfrei-Tornquist Zone and the Tornquist trend to the east (Mogensen & Jensen 1994; Thybo 2000; Mogensen & Korstgård 2003; Phillips et al. 2018) (Figure 17).

6.2 Implications for tectonic activity

The Mesozoic structural evolution of this area is relatively understudied (Jensen & Schmidt 1993; Phillips et al. 2018). Here we use inferences from our proposed geomorphological evolution of the Farsund Basin to place additional constraints on its tectono-stratigraphic evolution along with more regional tectonics.

The depositional limit of the Zechstein salt reflects relative structural highs present at the time of deposition (Figure 1). Onlapping of the salt onto the southern margin of the Farsund Basin indicates that, at that time, the area to the north formed part of the Stavanger Platform, prior to later activity along the Fjerritslev North and South faults. This is in agreement with structural observations that the Farsund Basin did not exist in its present form until the Early Cretaceous (See Phillips et al. 2018). An abrupt step of c. 7 km is observed in the limit across NS2 (Figure 1). This step may reflect pre-existing topography within the basin at the time of deposition, post-depositional modification and translation of the boundary due to later fault activity, or a combination of both. NS2, along with other N-S striking faults may have been active during the Carboniferous-Permian extensional event (Heeremans & Faleide 2004; Heeremans et al. 2004), although due to a lack of imaging at depth within our seismic data, we are unable to confirm this. Pre-existing fault-related relief could cause such a step in the depositional limit of mobile salt (Clark et al. 1998); similar steps are observed along-strike relating to the Stavanger Fault system (Figure 1) (Jackson & Lewis 2013). Additionally, the limit of the salt basin may have been modified post-deposition, perhaps relating to Early Jurassic sinistral strike-slip activity (Phillips et al. 2018).

East-trending fluvial channels within the Bryne Formation were, at least in part, controlled by the presence of thin-skinned, salt detached faults. A key observation is that these E-trending channels are not influenced by the major E-W striking faults, in particular the Fjerritslev South Fault, that delineate the present-day morphology of the basin. This concurs with structural observations, i.e. the lack of syn-kinematic pre-Cretaceous strata (Figure 3, 6), that the E-W faults were not active and had no surface expression at this time. The widening of fluvial channels across NS2 occurs across a subtle topographic gradient, interpreted as the paleo-shoreline. This topographic gradient may be related to differential compaction of underlying Triassic strata across NS2.

East-trending structures also have negligible influence on the formation and morphology of features within the Sandnes Formation. Patch reef morphology is unchanged across the E-W striking Fjerritslev North and South Faults, indicating that they grew in similarly shallow water depths (Figure 10) (Kendall & Schlager 1981). Conversely, patch reef morphology changes markedly across N-S striking faults, from short, wide reefs on the footwall, to tall, narrow reefs on the hangingwall (Figure 9, 10). Water depth has previously been shown to be a key factor in determining carbonate facies and patch reef morphology, with shallower water depths associated with shorter, wider reef morphologies (Brock et al. 2008), and favouring the formation of patch reefs over more continuous ridges (Colpaert et al. 2007; Purkis et al. 2015). Thus, we infer this change in reef morphology represents a change in water depth associated with the aforementioned topographic gradient across NS2 (Figure 9). Those patch reefs that grow in the slightly deeper water environment, i.e. the hangingwall of NS2, exhibit catch-up growth as they attempt to reach shallower depths, forming tall, narrow structures (Kendall & Schlager 1981; Schlager 1981; Saqab & Bourget 2016). On the other hand, the wider patch reefs situated at shallow water level, i.e. the footwall of NS2, have no requirement for this catch-up growth and undergo keep-up growth,

preferentially growing laterally, forming shorter, wider structures (Brock et al. 2008; Saqab & Bourget 2016). The occurrence of this catch-up/keep-up growth mechanism indicates that the growth of these structures was sensitive to water depth, and therefore that they formed as tropical carbonate reefs, as opposed to cool-water carbonates or carbonate mud mounds (Schlager 2000). Late Jurassic ocean temperatures were relatively equilibrated across the Tethyan Ocean, allowing tropical reefs to form across a large latitude range, including the Farsund Basin (Leinfelder 1994).

Following the deposition of the Egersund and Tau formations, a series of southwards prograding basin-floor fans were deposited in the Farsund Basin, forming part of the Upper Jurassic Sauda Formation. Fan geometry appears unaffected by any underlying relief, with the Fjerritslev North and South faults now cross-cutting fans. As the fans are now offset, this implies that no fault-related topography was present at the time of deposition and that the fans were deposited in a relatively unconfined setting (Somme et al. 2013; Zhang et al. 2016). The lack of Upper Jurassic fan systems across the footwall of the Fjerritslev South Fault may be due to erosion following post-depositional fault activity and sub-aerial exposure of the footwall. Based on this, we infer that activity along the E-W Fjerritslev North and South faults in the Farsund Basin began in the Early Cretaceous, following the deposition of the offshore fans. Conversely, fault activity within the Egersund Basin started earlier, in the latest Jurassic, affecting the thickness and distribution of different facies (Mannie et al. 2014; Mannie et al. 2016). In the Farsund Basin, this likely corresponds to the same extensional event, with the age of the offshore fans straddling the Jurassic/Cretaceous boundary.

The Sauda Formation represents an input of sandstone deposited during an overall net marine transgression (Mannie et al. 2016). This input of clastic material, both in the Farsund Basin and offshore west Norway (Somme et al. 2013), corresponded to the late pre-rift to peak-syn-rift stage of Late Jurassic-Early Cretaceous extension (Brun & Tron 1993; Bell et

al. 2014). The Early Cretaceous succession within the Farsund Basin predominately consists of relatively deep marine sediments. Deposition of these sediments was associated with a deepening of the Farsund Basin relating to Early Cretaceous tectonic activity (Mogensen & Jensen 1994). This likely represents the same regional rift event documented to the west, responsible for the deposition of the Hardangerfjord Delta sequence, although this event may be regionally diachronous (Somme et al. 2013; Mannie et al. 2016).

6.3 Petroleum system applications

In constraining the geomorphological evolution of the Farsund Basin, we have also identified a series of potential carbonate and clastic reservoirs that may form part of viable petroleum systems. Channels identified within the Bryne Formation (Figure 7) are likely composed of fluvial sandstones (Ryseth et al. 1998). In addition, carbonates, including patch reefs such as those identified within the Sandnes Formation (Figure 9, 10), and offshore deltas akin to those within the Sauda Formation (Figure 11, 12, 15) have previously been shown to represent viable petroleum reservoirs (Montgomery 1996; Moore 2001; Saller et al. 2008).

The reservoir potential of the Sandnes Formation patch reefs is complicated due to distinguishing between primary and secondary porosity within the reefs themselves (Enos & Sawatsky 1981). Original porosity within carbonates can be enhanced through dissolution of the host material, or alternatively, may be destroyed and infilled by secondary cementation. This secondary porosity is dependent on a number of different factors. Typically, patch reefs consist of a cemented core containing negligible porosity, with a less cemented, more porous surrounding framework (Enos & Sawatsky 1981). The high amplitude core and lower amplitude rim of the carbonate patch reefs as imaged in seismic data (Figure 9, 10a) may potentially reflect such a change in the degree of cementation, from a relatively compacted

and cemented core, to a more porous rim. These complications notwithstanding, working patch reef plays have been discovered, such as the Lime Valley Pinnacle Reef Play, in Texas, USA (e.g. Montgomery 1996).

Stratigraphic and structural traps and seals are present within the Farsund Basin. The Zechstein salt would act as a regional seal throughout large parts of the area. However, areas to the north of the depositional limit of the salt may allow vertical migration into the Jurassic section (Figure 1). The carbonate patch reefs and fluvial channel systems are largely overlain by and encased in shales of the Egersund and Tau formations (Figure 3, 5). In addition, the isolated nature of the fluvial systems and the patch reefs allow them to represent volumes with well-defined stratigraphic pinchouts at the margins. The lateral terminations of the Upper Jurassic fan systems also represent stratigraphic pinchout traps and are sealed by overlying Lower Cretaceous claystones and siltstones. Due to the main period of faulting along the E-W faults occurring following the deposition of the Jurassic interval, including these potential reservoir units (Figure 3, 6), a number of structural traps may also be present. Early Cretaceous faulting offsets and partitions the Upper Jurassic fans into a series of discrete potential reservoir units (Figure 16).

In addition to these reservoirs, a number of potential source rocks are present throughout the area, each of varying maturity and likelihood of viability. The organic-rich shales of the Tau Formation may be oil-mature in the centre of the Farsund Basin (Skjerven et al. 1983; Sørensen & Tangen 1995; Petersen et al. 2008). These correspond regionally to the Kimmeridge Clay and Draupne shales in the UK and Norwegian North Sea respectively, which represent key source rock intervals in each area. The Tau Formation shales may be able to act as a local source rock for the identified Jurassic reservoirs. Regionally, the Cambrian aged Alum shales, situated to the east of the area (Petersen et al. 2008), may be mature and could act as a potential source rock in this region, although potential migration

pathways into the Jurassic interval in this area seem far-fetched. Through constraining its geomorphological evolution we have identified and mapped key components of the petroleum system within the Farsund Basin, and have shown how seismic attribute driven interpretation can aid the imaging and mapping of petroleum systems in frontier areas.

7 Conclusions

In this study we have used a seismic attribute-driven approach to determine the geomorphological evolution of the Triassic-Jurassic succession in the Farsund Basin, offshore south Norway. Having established this local evolution, we link this to the tectono-stratigraphic evolution of the wider area and assess the viability of any potential petroleum systems. Overall, we find that:

1. The depositional limit of mobile Zechstein salt trends E-W across the southern margin of the Farsund Basin, onlapping the edge of the Stavanger Platform at the time of its deposition. A step in the depositional limit likely reflects base-salt relief relating to a pre-existing fault scarp, but may also be a result of post-depositional modification of the basin.
2. The geomorphological evolution of the Farsund Basin reflects an overall marine transgression, documented through the identification of fluvial river systems of the Middle Jurassic Bryne Formation, shallow marine patch reefs developed within the Sandnes Formation, and Late Jurassic aggrading delta lobes within the Sauda Formation.
3. The morphology of the identified geomorphological features offer insights into the paleo-geographical setting of the basin. Paleo-topography, formed as a result of differential compaction across previously active faults, represents the paleo-shoreline and reflects a change in water depth throughout the deposition of the Bryne and

Sandnes formations. The Upper Jurassic fan systems are unaffected by, and were therefore deposited prior to, the onset of faulting within the Farsund Basin

4. The tectono-stratigraphic evolution of the Farsund Basin differs markedly to that of the Egersund Basin to the west, due to the presence of a partition between the two areas. This partition is formed of structural highs corresponding to the Stavanger Platform and Lista Nose Fault Blocks offshore, and potentially the drainage divide onshore. These differing tectono-stratigraphic evolutions between the two areas reflects a difference in their regional tectonic settings, the evolution of the Egersund Basin area is controlled by Caledonian orogeny and orogenic collapse related structures, and the Farsund Basin by the underlying Sorgenfrei-Tornquist Zone.
5. Through this seismic geomorphological analysis we have identified a series of potential reservoirs, including fluvial systems, carbonate patch reefs, and offshore deltaic fans, which along with seals and local sources within the Tau Formation, may form parts of working petroleum systems within the area.

This study showcases how seismic attributes and seismic geomorphological analysis can be used to determine the tectono-stratigraphic evolution of rift basins. These techniques are able to identify potential petroleum systems, representing a vital tool for the exploration of relatively underexplored frontier basins, and also offer insights into the structural evolution and wider tectonic settings of relatively underexplored basins.

Acknowledgements

This contribution forms part of the MultiRift project, funded by the Research Council of Norway's PETROMAKS programme (project number 215591) and Statoil to the University of Bergen and partners Imperial College, University of Manchester and University of Oslo.

The authors would like to thank PGS for allowing us to show and use the seismic data

presented in this study and GeoTeric for providing us with academic licences for the software to undertake the spectral decomposition in the project. We would also like to thank Schlumberger for providing academic licences of the Petrel software to Imperial College.

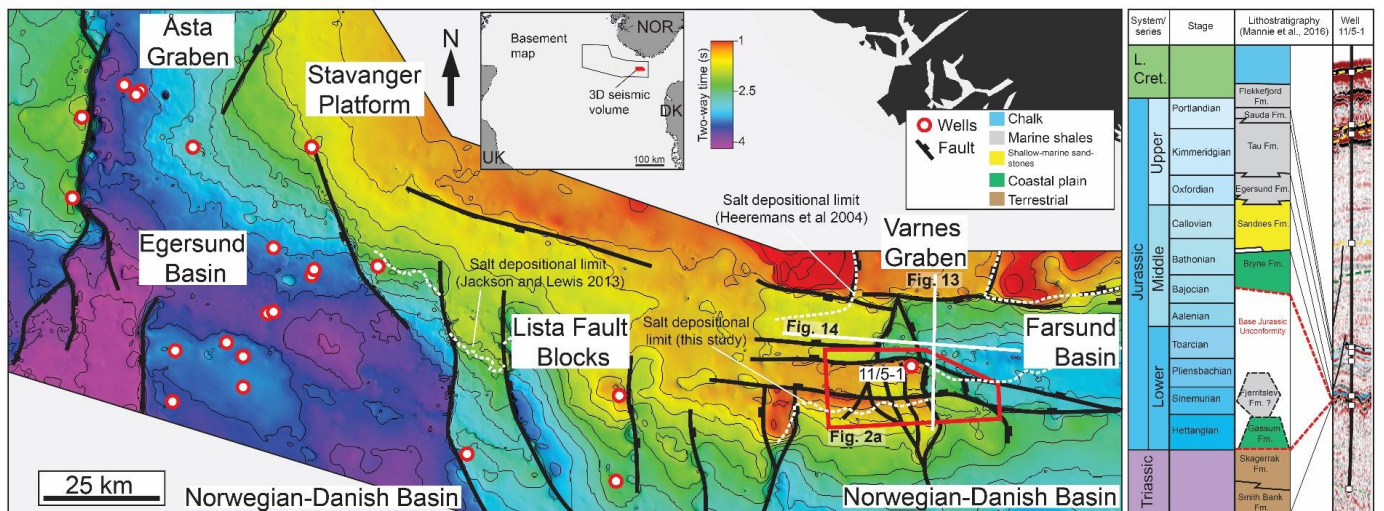


Figure 1 - A) TWT structure map showing the acoustic basement (Base upper Permian/Zechstein salt) surface throughout the study area. Red circles represent wells throughout the area, note the high density of well coverage in the Egersund Basin compared to the Farsund Basin. Also shown are the location of the 3D seismic survey referred to in this study and the salt depositional limits proposed by Jackson and Lewis (2013), Heeremans et al. (2014) and this study. B) Jurassic stratigraphic column. Lithostratigraphy from Mannie et al. (2016), focused on well data from the Egersund Basin, is contrasted against seismic data around well 11/5-1, located within the Farsund Basin. Note the lack of Triassic and Middle-Lower Jurassic strata in well 11/5-1.

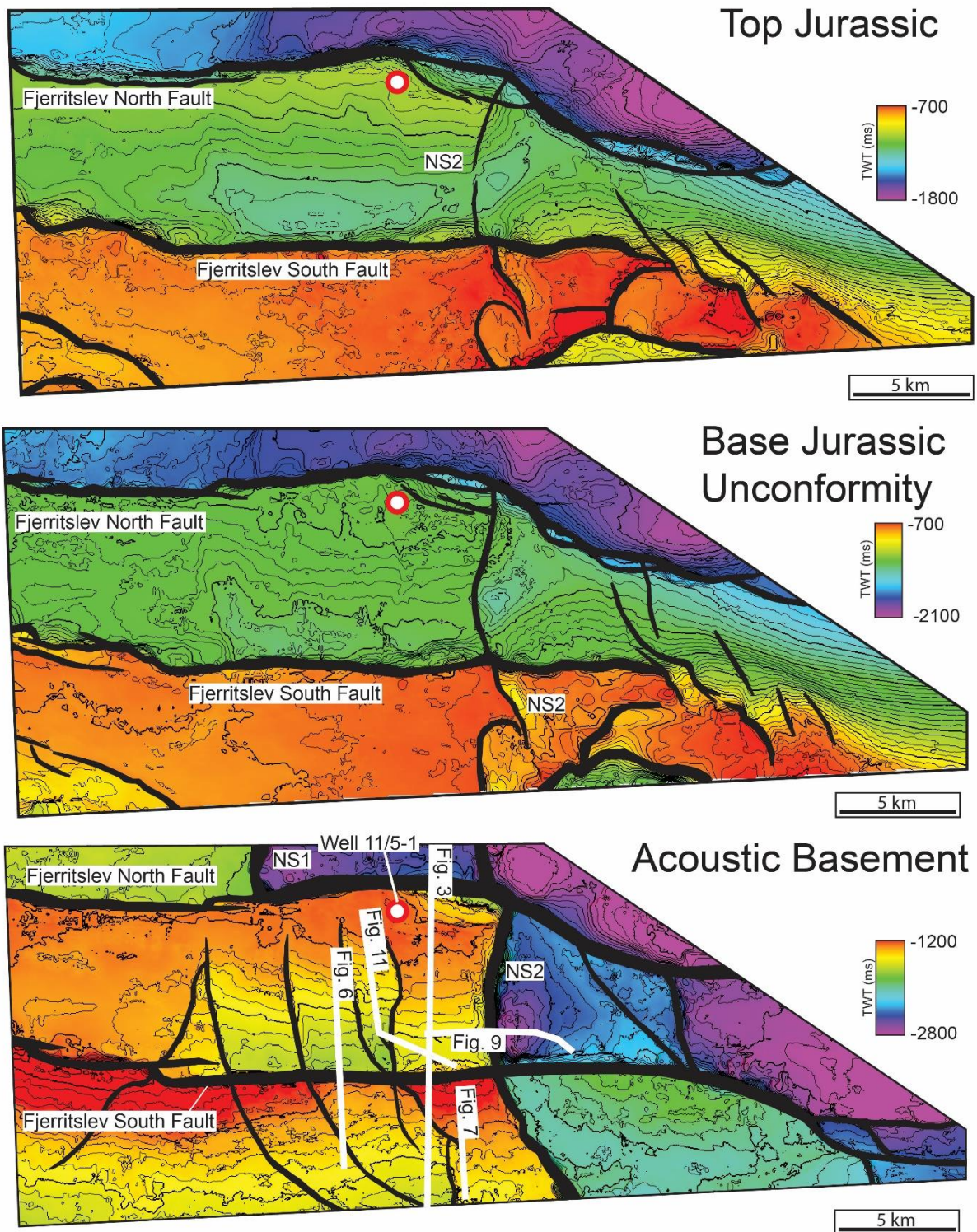


Figure 2 – TWT structure maps of key stratigraphic horizons within the 3D volume located over the southern margin of the Farsund Basin. See Figure 1a for location and Figure 1b for the stratigraphic ages of horizons. A) TWT structure map of the Top Jurassic surface, dominated by the E-W striking Fjerritslev North and Fjerritslev South Faults. Also present is the N-S striking NS2 fault. B) TWT structure map of the stratigraphically deeper Base Jurassic Unconformity. C) TWT structure map of the base Zechstein salt acoustic basement surface. This surface is dominated by a series of N-S and E-W striking faults.

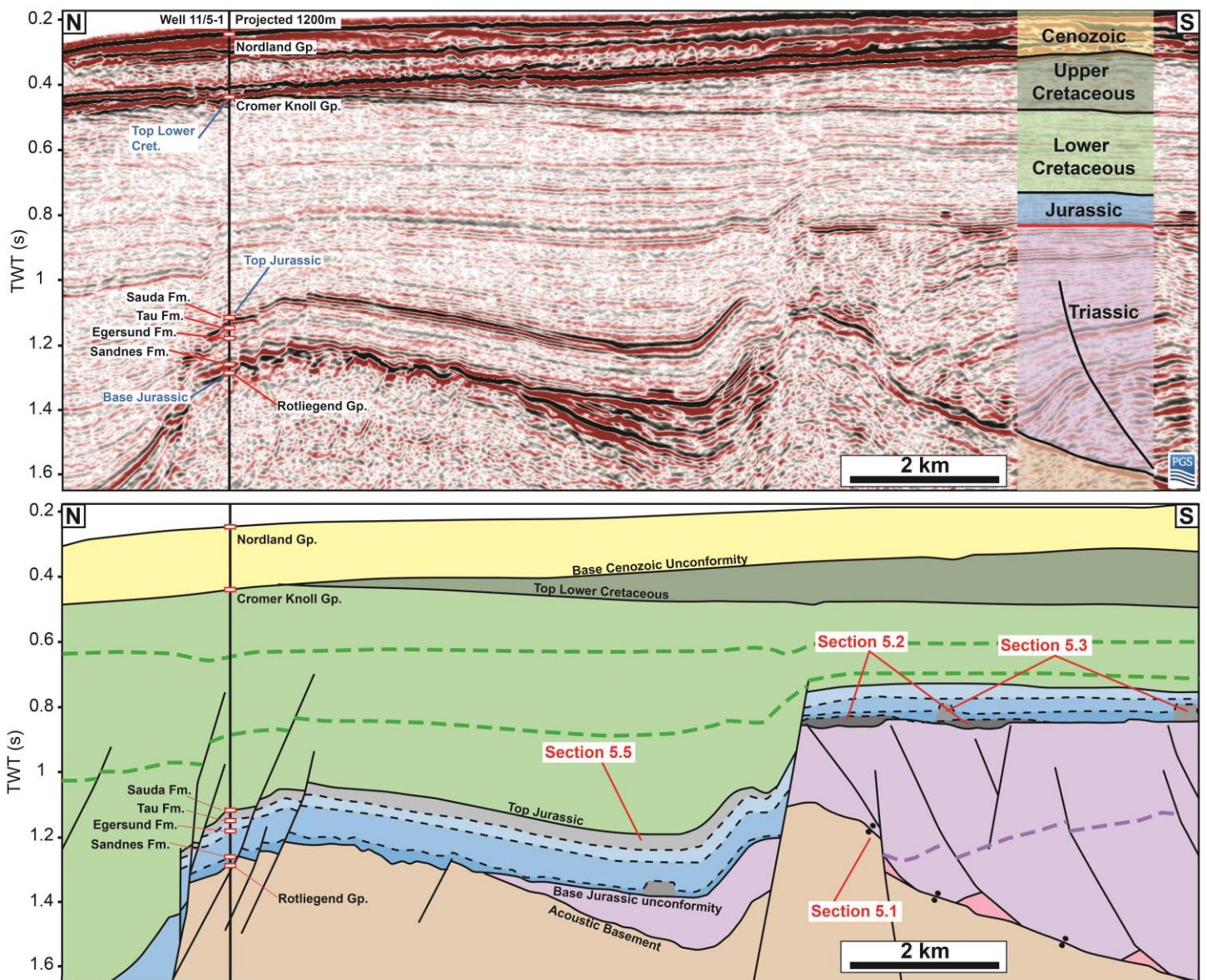


Figure 3 – Uninterpreted and interpreted seismic sections across the study area showing the Triassic and Jurassic intervals. Note that the Jurassic interval appears restorable across the Fjerritslev South Fault, indicating that fault activity occurred later, during the Early Cretaceous. Also, the upper Jurassic interval appears eroded from the footwall of the Fjerritslev South Fault. Structures analysed in sections 5.1, 5.2, 5.3 and 5.5 are labelled on the interpreted section. See Figure 2 for location.

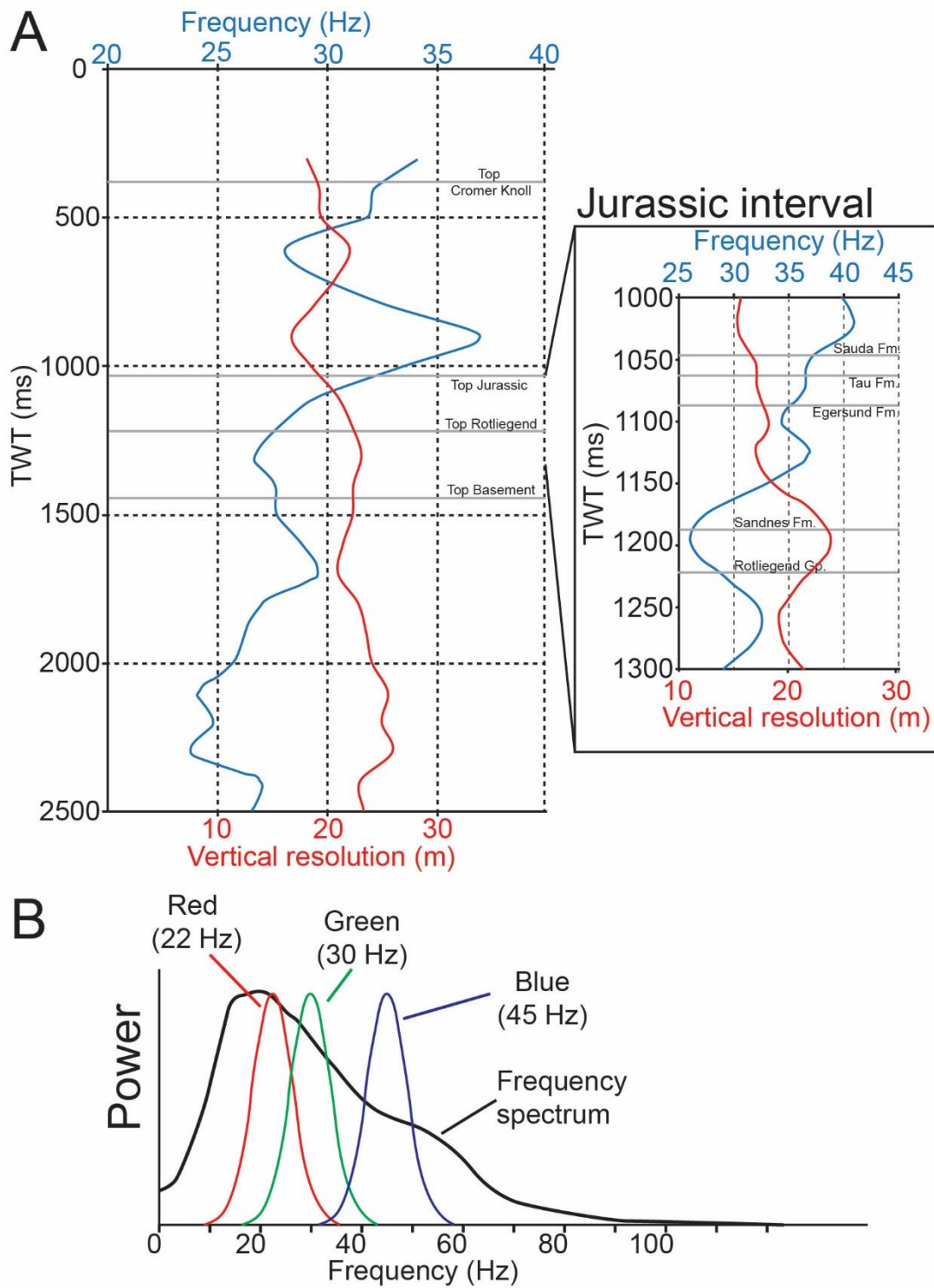


Figure 4 – A) Frequency vs depth throughout the Farsund Basin in the vicinity of the 11/5-1 well. Inset- Closeup of the changing frequency with depth within the Jurassic interval. Frequency was calculated within a 3-point moving average. Vertical resolution was also calculated at various depths. B) Frequency spectrum for the 3D seismic volume. Also shown are the extracted frequency bins combined to create the spectral decomposition seismic attribute.

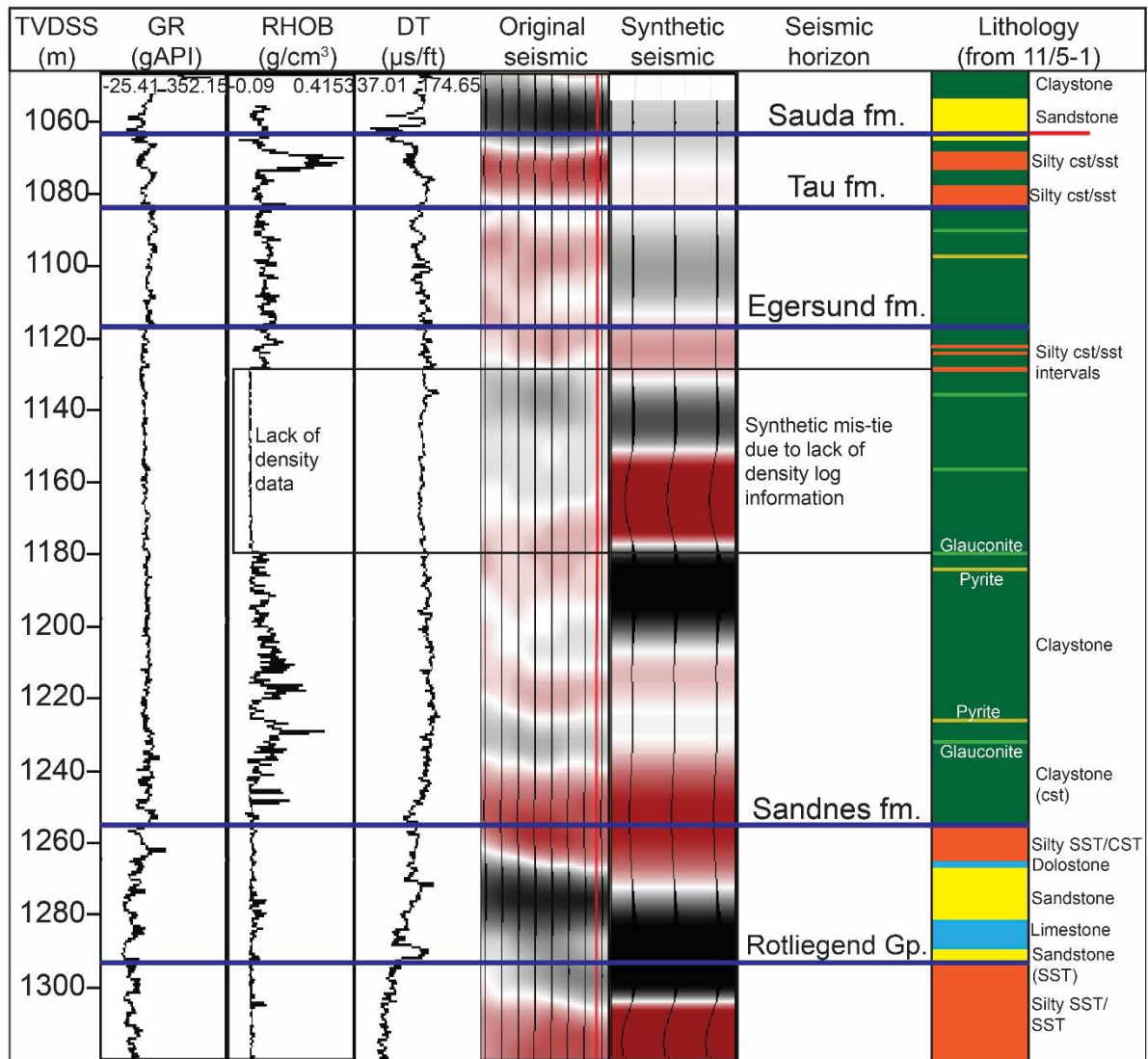


Figure 5 – Well log information and synthetic seismic for the Jurassic interval of well 11/5-1. Synthetic seismic section was created using the RHOB and DT wireline logs of the well. A lack of density data at around 1130-1180m results in a major discrepancy between the original and synthetic seismic data. Otherwise, the synthetic provides a good match to the original seismic at the Rotliegend Group and Sandnes Formation intervals, as well as the Sauda Formation.

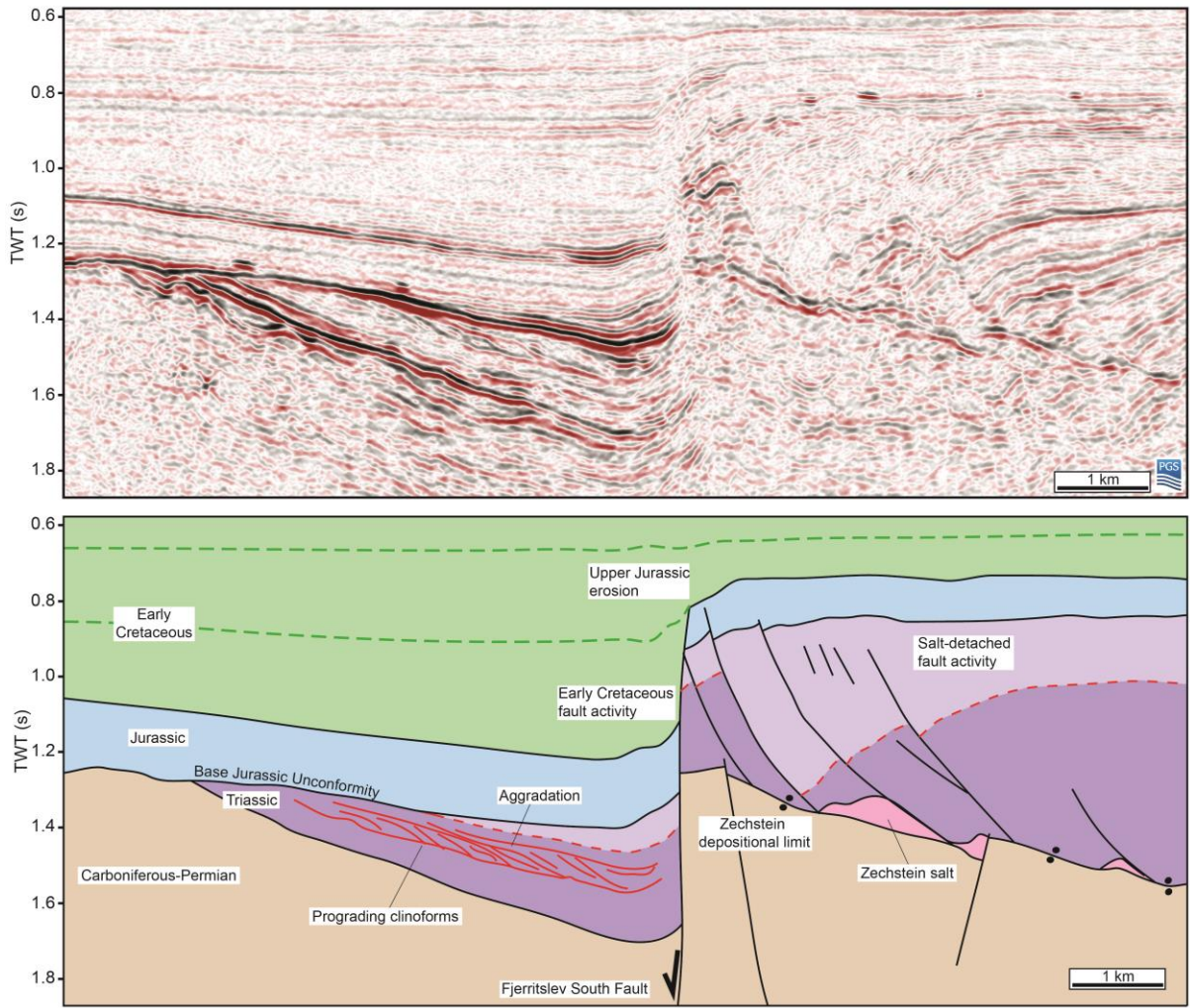


Figure 6 – Uninterpreted and interpreted seismic section showing the northwards limit of thin-skinned, salt-detached faulting marking the northern depositional limit of mobile salt. Also note that an undeformed clinoform interval progrades southwards before being offset by thin-skinned faulting to the south. See Figure 2 for location.

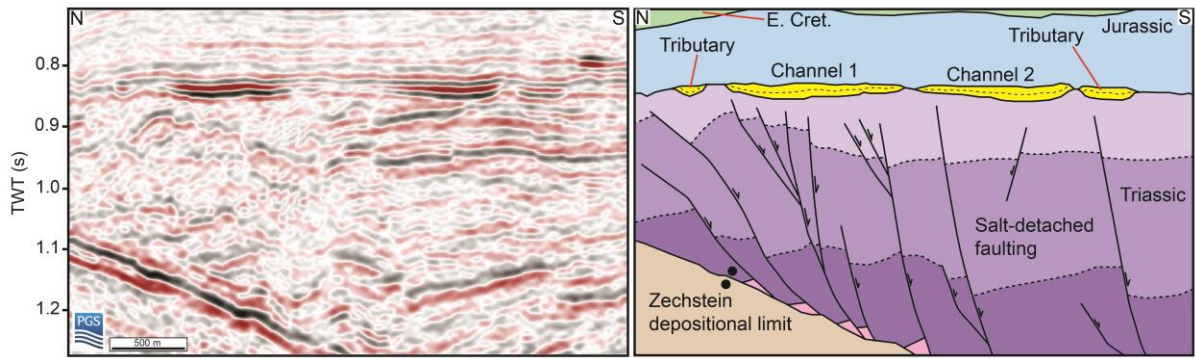


Figure 7 – Uninterpreted and interpreted N-trending seismic sections across the southern margin of the Farsund Basin, see Figure 2 for location. Two distinct high-amplitude features can be observed at the base of the Jurassic interval corresponding to channel systems. Note that the channel systems are predominately situated within the hangingwalls of the thin-skinned, salt-detached faults.

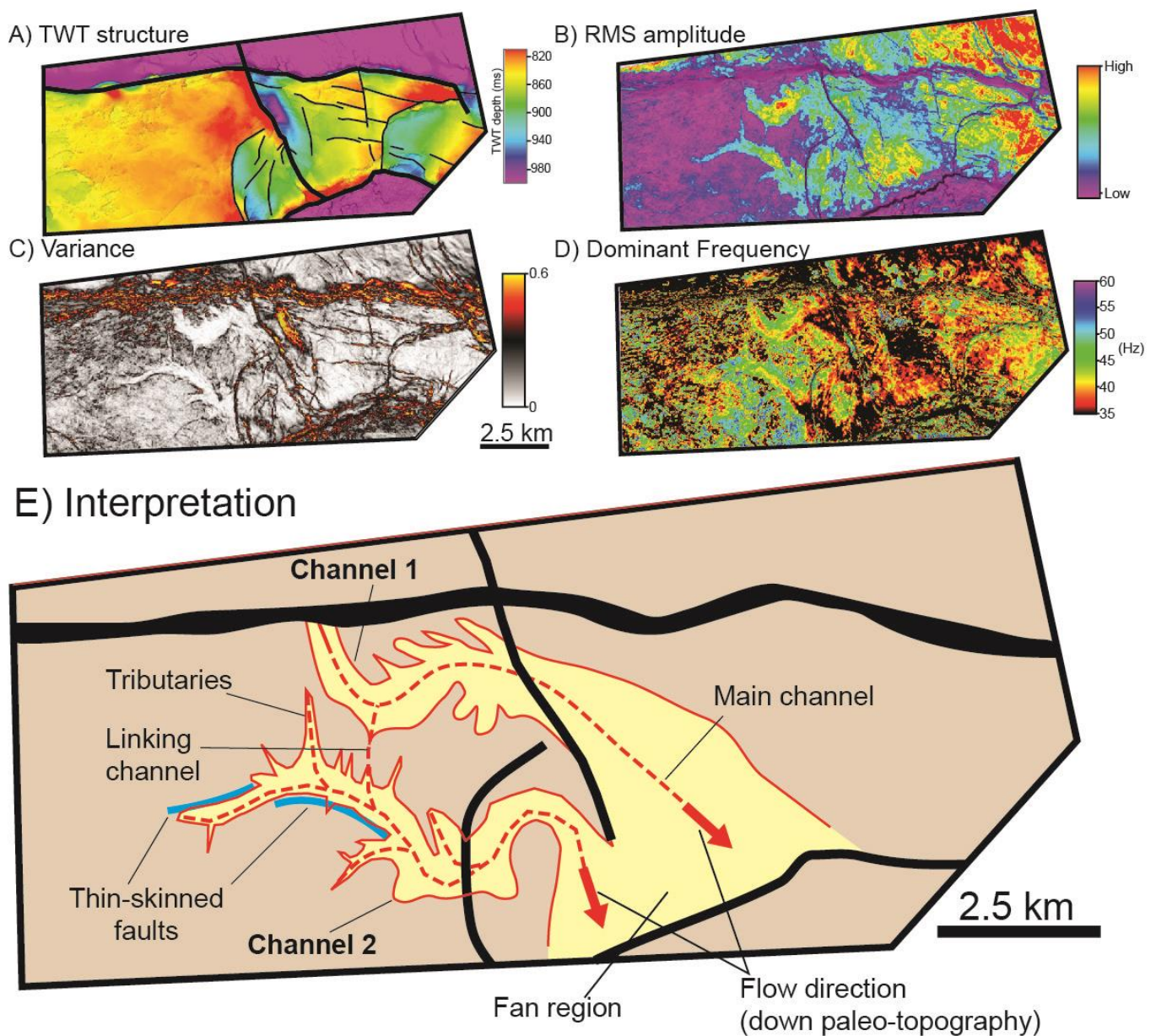


Figure 8 – Seismic attribute maps of the southern margin of the Farsund Basin, calculated in a 25 ms TWT window below the top of the high amplitude structures. A) TWT structure map of the area, located at the intersection of the NS2 and Fjerritslev South faults. B) RMS amplitude seismic attribute, highlighting two high amplitude E-trending channel-like features, widening across NS2. C) Variance seismic attribute, further delineating the margins of the structures. D) Dominant frequency attribute, showing the overall geometry of the features and showing a decrease in frequency in the centre of the structure towards the east. E) Interpretation, based on the seismic attributes above, of these features as a fluvial channel system, widening into a more deltaic environment across NS2.

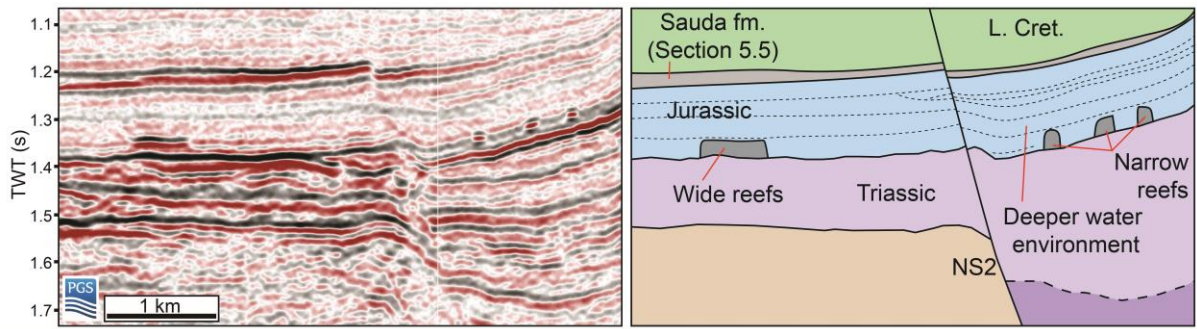


Figure 9 – Uninterpreted and interpreted seismic section showing a series of discrete high amplitude structures within the Sandnes Formation. A wider, shorter structure is present on the footwall of NS2, with taller, narrower structures on the hangingwall. See Figure 2 for location.

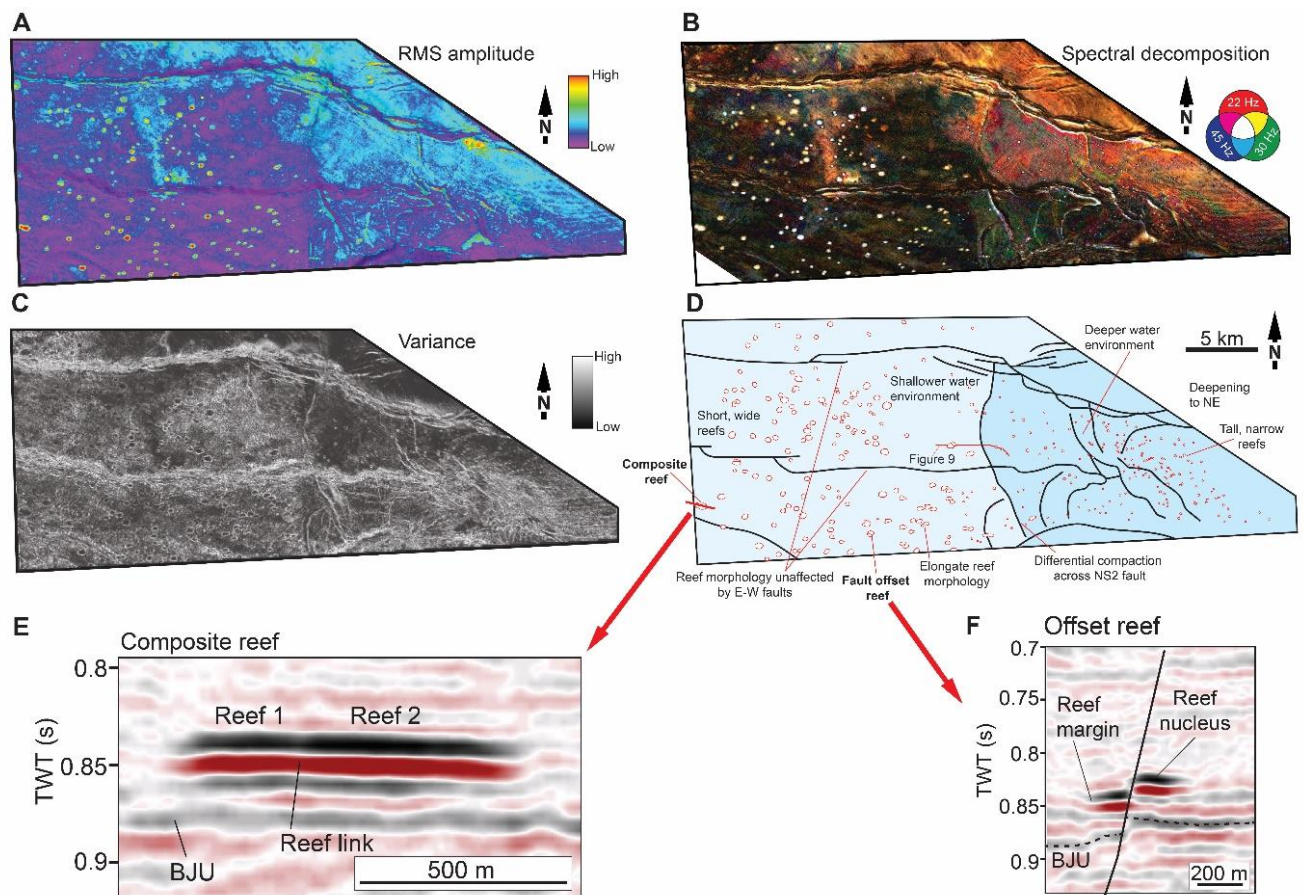


Figure 10 – Compilation of seismic attributes extracted from a 50 ms TWT window above the Base Jurassic Unconformity across the whole of the 3D seismic volume, see Figure 1 for location. A) RMS amplitude highlighting high amplitude, sub-circular structures. B) Spectral decomposition, highlighting sub-circular structures, including those on the hangingwall of NS2. C) Variance, showing that the structures contain few internal discontinuities. D) Interpretation of the area, showing wider sub-circular structures, interpreted as carbonate patch reefs, on the footwall of NS2 and smaller structures on the hangingwall. E) Seismic section showing a composite reef, formed through the radial growth and coalescence of two individual reefs. See Figure 10d for location. F) Seismic section showing a reef offset by later faulting, implying a brittle nature. See Figure 10d for location.

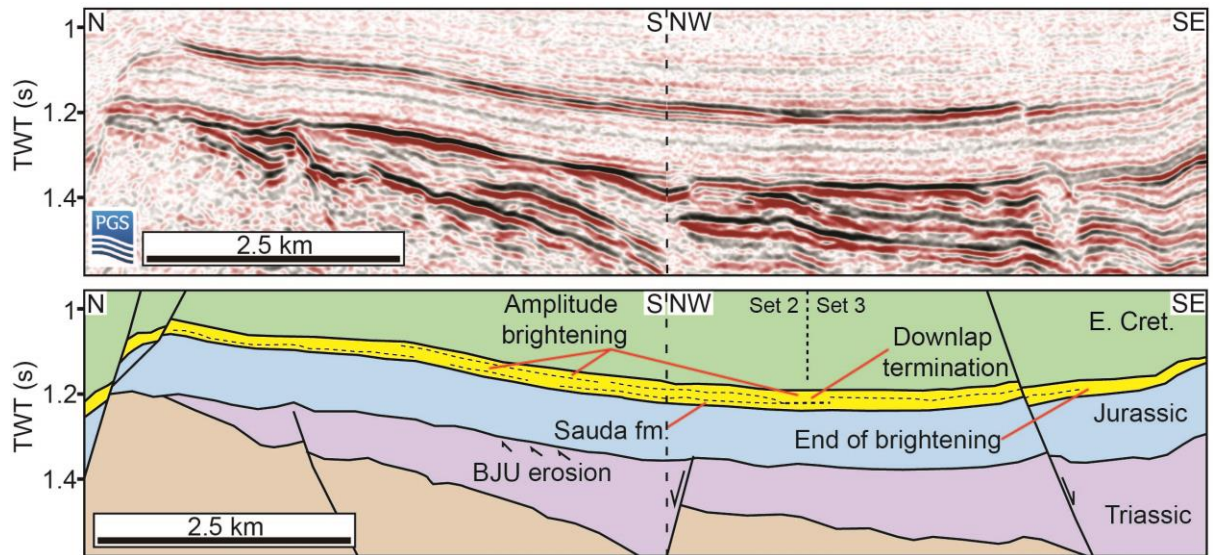


Figure 11 – Uninterpreted and interpreted seismic section showing lateral amplitude changes within the upper Jurassic Sauda Formation. Two distinct sets can be identified (Set 2 and Set 3), defined by downlap terminations of clinoform structures. See Figure 2 for location.

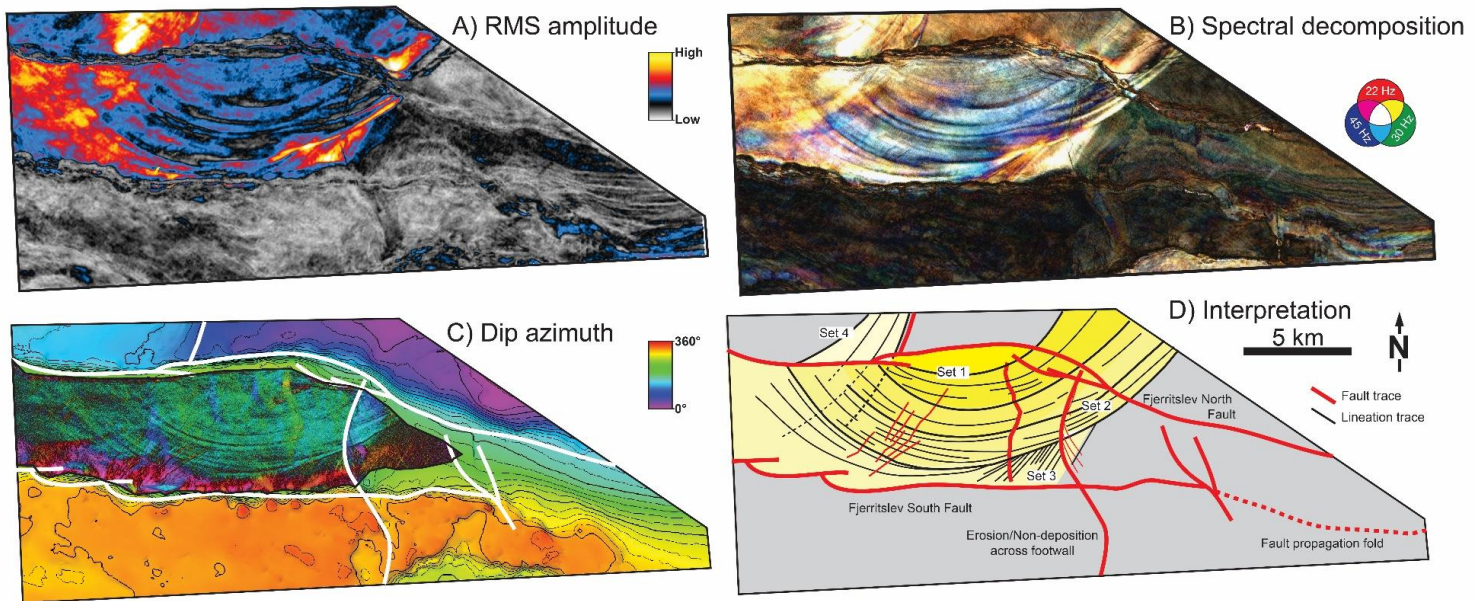


Figure 12 – Seismic attribute maps across the 3D seismic volume extracted from a window between the top and the base of the high amplitude package (see Figure 10). A) RMS amplitude attribute map showing a series of concave to the south, curvilinear high amplitude lineations. B) Spectral decomposition seismic attribute, highlighting internal lineation geometries and relationships between individual sets. C) Dip azimuth of the lineations, further highlighting the curvilinear and discordant nature of the lineation sets. D) Interpretation of the lineation sets. The curvilinear lineations are arranged into a series of discordant sets that truncate each other at low angles. A further, concave-to-the-east lineation set is present along the footwall of NS1. Note that the lineations are not present across the footwall of the Fjerritslev South Fault and do not appear to be influenced by the Fjerritslev North Fault.

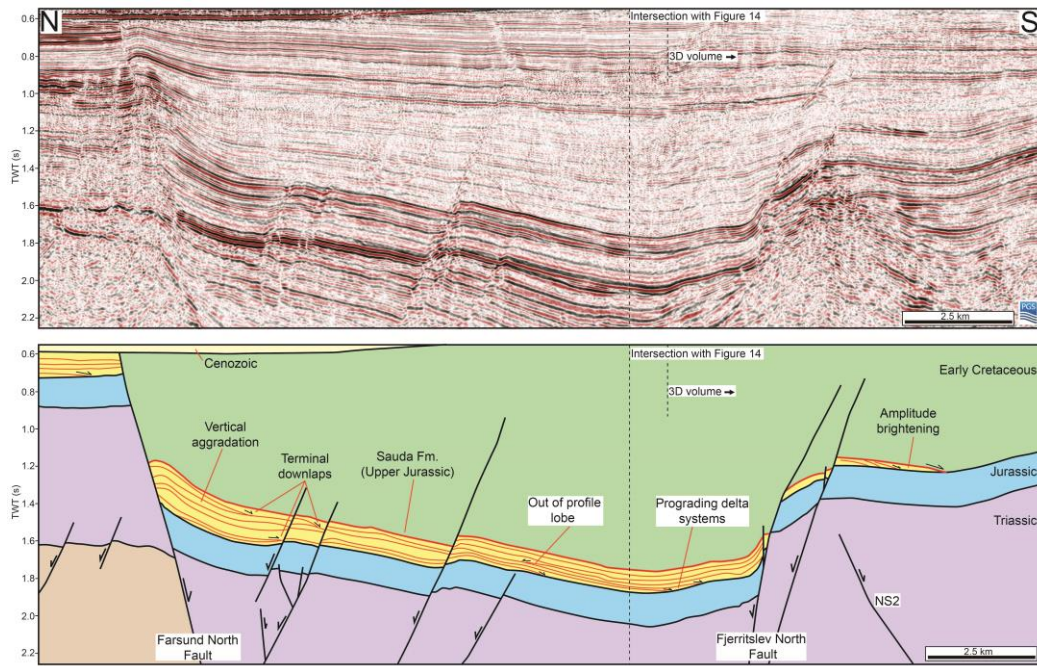


Figure 13 – Uninterpreted and interpreted N-S oriented seismic section across the Farsund Basin. See Figure 1 for location. The area also imaged in the 3D volume is situated to the south. A series of deltaic systems are identified prograding southwards and aggrading and stacking atop one another, as evidenced by downlap terminations.

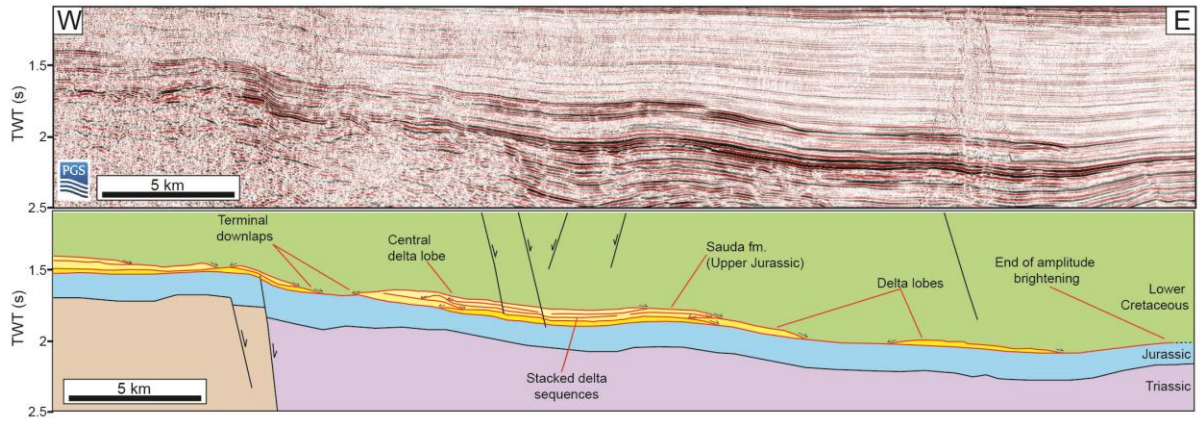


Figure 14 – Uninterpreted and interpreted E-W oriented seismic section. See Figure 1 for location. Three discrete deltaic fans can be identified across the area, with lateral downlap terminations observed either side. These fans appear to thicken towards the west.

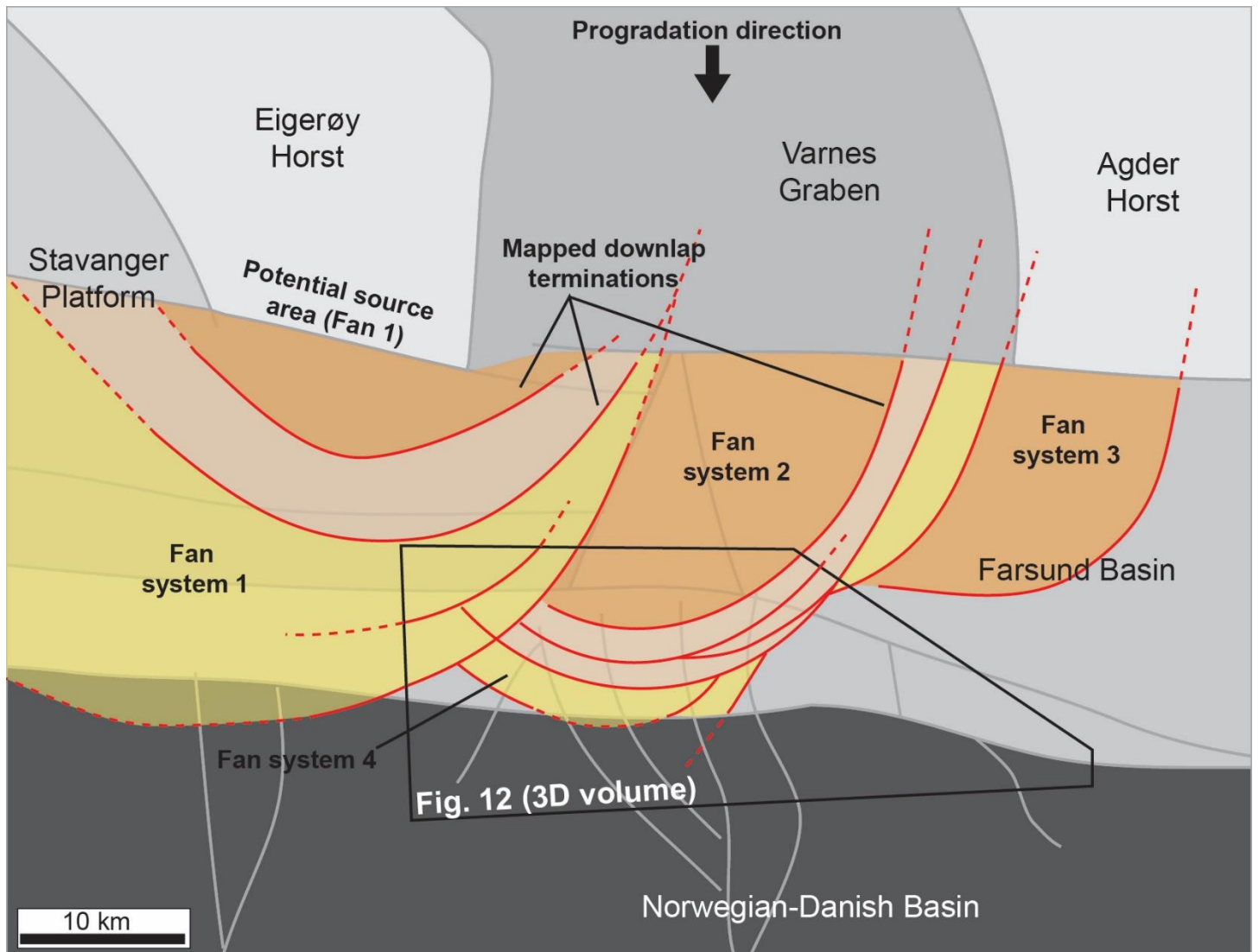


Figure 15 – Compilation and map-view geometry of the deltaic lobes within the Farsund Basin. The location of the 3D volume is shown by the black polygon whilst grey lines mark the major faults. Fan geometries are based on lateral downlap terminations (see Figure 13 and 14). These downlap terminations correspond to the along-strike continuations of the lineations identified within the 3D volume. A series of deltaic fans are identified, prograding from the north and stacking progressively towards the west.

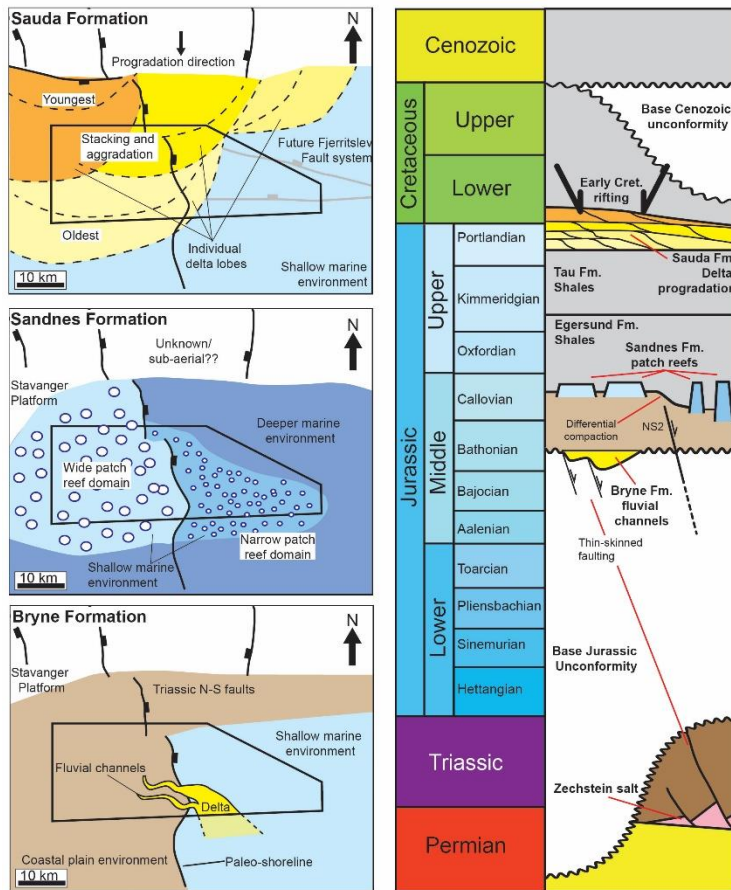


Figure 16 –Left. A) Coastal plain-shallow marine environment during the deposition of the Bryne Formation with eastwards flowing fluvial systems widening into a more deltaic environment across NS2. B) Patch reef development within a sheltered shallow marine environment during the deposition of the Sandnes Formation. Wide, short patch reefs present in shallower water pass eastwards into a deeper environment, consisting of tall, narrow patch reefs, across the NS2 fault. C) Progradation of shallow marine deltaic systems from the north during the Late Jurassic and the deposition of the Sauda Formation. Right – Tectono-stratigraphic chart showing the local evolution of the Farsund Basin as evidenced in this study.

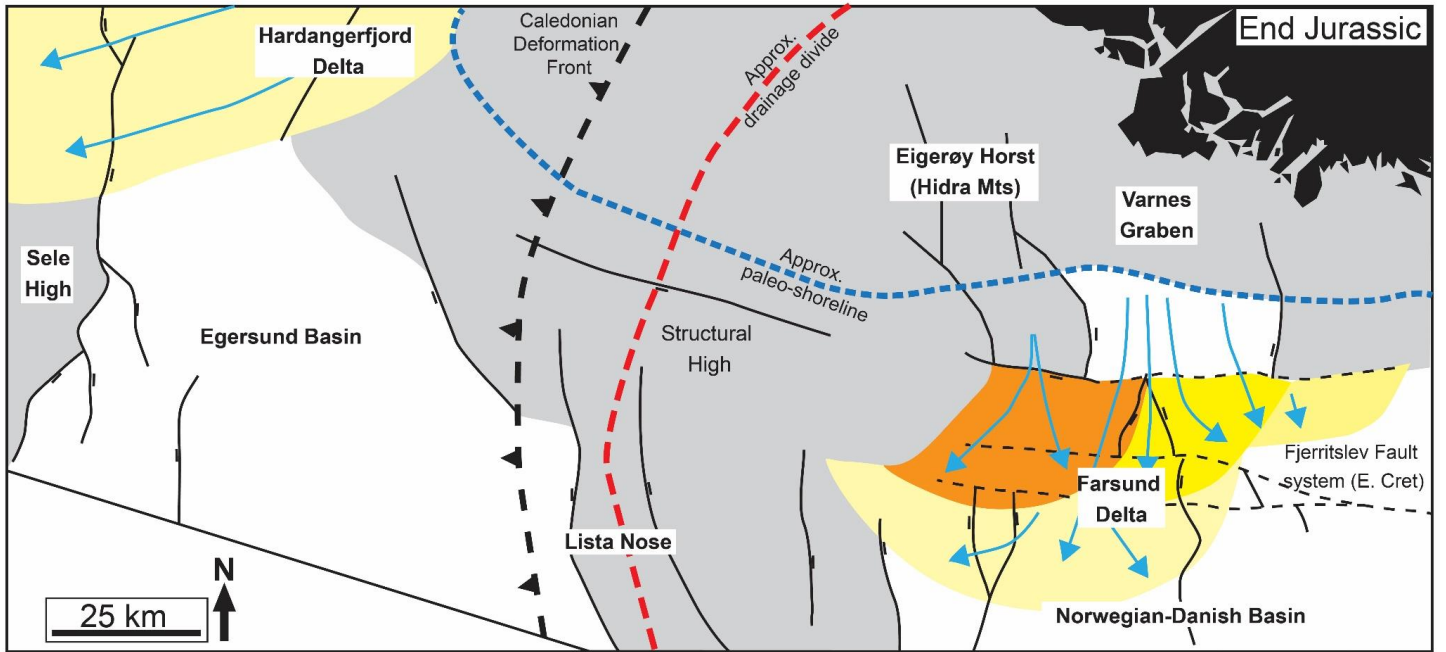


Figure 17 – Regional tectono-stratigraphic setting of the study area during the Late Jurassic and deposition of the Sauda Formation. The Farsund Basin is dominated by the progradation of the Farsund Delta, whereas the Egersund Basin is dominated by the Hardangerfjord Delta, with the two areas separated by the intervening structural high of the Stavanger Platform and Lista Nose Fault Blocks.

References

- Agirrezabala, L.M., Kiel, S., Blumenberg, M., Schäfer, N. & Reitner, J. 2013. Outcrop analogues of pockmarks and associated methane-seep carbonates: A case study from the Lower Cretaceous (Albian) of the Basque-Cantabrian Basin, western Pyrenees. *Palaeogeography, Palaeoclimatology, Palaeoecology*, **390**, 94-115, <http://doi.org/10.1016/j.palaeo.2012.11.020>.
- Andresen, K.J., Huuse, M., Schodt, N.H., Clausen, L.F. & Seidler, L. 2011. Hydrocarbon plumbing systems of salt minibasins offshore Angola revealed by three-dimensional seismic analysis. *AAPG Bulletin*, **95**, 1039-1065.
- Andsbjerg, J. 2003. Sedimentology and sequence stratigraphy of the Bryne and Lulu formations, middle Jurassic, northern Danish Central Graben. *The Jurassic of Denmark and Greenland. Geological Survey of Denmark and Greenland Bulletin*, **1**, 301-347.
- Bell, R.E., Jackson, C.A.L., Whipp, P.S. & Clements, B. 2014. Strain migration during multiphase extension: Observations from the northern North Sea. *Tectonics*, **33**, 1936-1963, <http://doi.org/10.1002/2014TC003551>.
- Billy, J., Robin, N., Hein, C.J., Certain, R. & FitzGerald, D.M. 2014. Internal architecture of mixed sand-and-gravel beach ridges: Miquelon-Langlade Barrier, NW Atlantic. *Marine Geology*, **357**, 53-71, <http://doi.org/10.1016/j.margeo.2014.07.011>.
- Brock, J.C., Palaseanu-Lovejoy, M., Wright, C.W. & Nayegandhi, A. 2008. Patch-reef morphology as a proxy for Holocene sea-level variability, Northern Florida Keys, USA. *Coral Reefs*, **27**, 555-568.
- Brown, A.R. 2011. *Interpretation of three-dimensional seismic data*. Society of Exploration Geophysicists and American Association of Petroleum Geologists.
- Brun, J.-P. & Tron, V. 1993. Development of the North Viking Graben: inferences from laboratory modelling. *Sedimentary Geology*, **86**, 31-51.
- Cartwright, J. & Huuse, M. 2005. 3D seismic technology: the geological 'Hubble'. *Basin Research*, **17**, 1-20, <http://doi.org/10.1111/j.1365-2117.2005.00252.x>.
- Chopra, S. & Marfurt, K.J. 2008. Emerging and future trends in seismic attributes. *The Leading Edge*, **27**, 298-318, <http://doi.org/10.1190/1.2896620>.
- Christensen, J.E. & Korstgård, J.A. 1994. The Fjerritslev Fault offshore Denmark - salt and fault interactions. *First Break*, **12**.
- Clark, J.A., Stewart, S.A. & Cartwright, J.A. 1998. Evolution of the NW margin of the North Permian Basin, UK North Sea. *Journal of the Geological Society*, **155**, 663-676, <http://doi.org/10.1144/gsjgs.155.4.0663>.
- Colpaert, A., Pickard, N., Mienert, J., Henriksen, L.B., Rafaelsen, B. & Andreassen, K. 2007. 3D seismic analysis of an Upper Palaeozoic carbonate succession of the Eastern Finnmark Platform area, Norwegian Barents Sea. *Sedimentary Geology*, **197**, 79-98, <http://doi.org/10.1016/j.sedgeo.2006.09.001>.
- Coward, M.P., Dewey, J.F., Hempton, M. & Holroyd, J. 2003. Tectonic evolution. In: Evans, D., Graham, C., Armour, A. & Bathurst, P. (eds) *The Millennium Atlas: petroleum geology of the central and northern North Sea*, Geological Society of London
- Davies, R.J. & Stewart, S.A. 2005. Emplacement of giant mud volcanoes in the South Caspian Basin: 3D seismic reflection imaging of their root zones. *Journal of the Geological Society*, **162**, 1-4, <http://doi.org/10.1144/0016-764904-082>.

- Dreyer, T., Whitaker, M., Dexter, J., Flesche, H. & Larsen, E. 2005. From spit system to tide-dominated delta: integrated reservoir model of the Upper Jurassic Sognefjord Formation on the Troll West Field. *Geological Society, London, Petroleum Geology Conference series*, **6**, 423-448, <http://doi.org/10.1144/0060423>.
- Eide, C.H., Klausen, T.G., Katkov, D., Suslova, A.A. & Helland-Hansen, W. 2017. Linking an Early Triassic delta to antecedent topography: Source-to-sink study of the southwestern Barents Sea margin. *GSA Bulletin*, <http://doi.org/https://doi.org/10.1130/B31639.1>.
- Enos, P. & Sawatsky, L.H. 1981. Pore networks in Holocene carbonate sediments. *Journal of Sedimentary Research*, **51**, 961-985, <http://doi.org/10.1306/212f7df1-2b24-11d7-8648000102c1865d>.
- Fichler, C., Henriksen, S., Rueslaatten, H. & Hovland, M. 2005. North Sea Quaternary morphology from seismic and magnetic data: indications for gas hydrates during glaciation. *Petroleum Geoscience*, **11**, 331-337, <http://doi.org/10.1144/1354-079304-635>.
- Færseth, R.B. 1996. Interaction of Permo-Triassic and Jurassic extensional fault-blocks during the development of the northern North Sea. *Journal of the Geological Society*, **153**, 931-944, <http://doi.org/10.1144/gsjgs.153.6.0931>.
- Glennie, K.W. 1997. Recent advances in understanding the southern North Sea Basin: a summary. *Geological Society, London, Special Publications*, **123**, 17-29, <http://doi.org/10.1144/gsl.sp.1997.123.01.03>.
- Glennie, K.W., Higham, J. & Stemmerik, L. 2003. Permian. In: Evans, D. (ed) *The Millenium Atlas: Petroleum geology of the Central and Northern North Sea*. The Geological Society of London
- Goldsmith, P.J., Rich, B. & Standring, J. 1995. Triassic correlation and stratigraphy in the South Central Graben, UK North Sea. *Geological Society, London, Special Publications*, **91**, 123-143, <http://doi.org/10.1144/gsl.sp.1995.091.01.07>.
- Hamar, G., Fjaeran, T. & Hesjedal, A. 1983. Jurassic stratigraphy and tectonics of the south-southeastern Norwegian offshore *Petroleum Geology of the Southeastern North Sea and the Adjacent Onshore Areas*. Springer, 103-114.
- Heeremans, M. & Faleide, J.I. 2004. Late Carboniferous-Permian tectonics and magmatic activity in the Skagerrak, Kattegat and the North Sea. *Geological Society, London, Special Publications*, **223**, 157-176.
- Heeremans, M., Faleide, J.I. & Larsen, B.T. 2004. Late Carboniferous -Permian of NW Europe: an introduction to a new regional map. *Geol Soc London, Special Publication*, **223**, 75-88.
- Holgate, N.E., Jackson, C.A.L., Hampson, G.J. & Dreyer, T. 2013. Sedimentology and sequence stratigraphy of the Middle–Upper Jurassic Krossfjord and Fensfjord formations, Troll Field, northern North Sea. *Petroleum Geoscience*, **19**, 237.
- Holgate, N.E., Hampson, G.J., Jackson, C.A.-L. & Petersen, S.A. 2014. Constraining uncertainty in interpretation of seismically imaged clinofolds in deltaic reservoirs, Troll field, Norwegian North Sea: Insights from forward seismic models of outcrop analogs. *AAPG Bulletin*, **98**, 2629-2663.
- Hovland, M., Talbot, M.R., Qvale, H., Olausson, S. & Aasberg, L. 1987. Methane-related carbonate cements in pockmarks of the North Sea. *Journal of Sedimentary Research*, **57**.
- Jackson, C.A.L. & Lewis, M.M. 2013. Physiography of the NE margin of the Permian Salt Basin: new insights from 3D seismic reflection data. *Journal of the Geological Society*, **170**, 857-860, <http://doi.org/10.1144/jgs2013-026>.

- Jackson, C.A.L., Chua, S.T., Bell, R.E. & Magee, C. 2013. Structural style and early stage growth of inversion structures: 3D seismic insights from the Egersund Basin, offshore Norway. *Journal of Structural Geology*, **46**, 167-185, <http://doi.org/10.1016/j.jsg.2012.09.005>.
- Jackson, C.A.L., Grunhagen, H., Howell, J.A., Larsen, A.L., Andersson, A., Boen, F. & Groth, A. 2010. 3D seismic imaging of lower delta-plain beach ridges: lower Brent Group, northern North Sea. *Journal of the Geological Society*, **167**, 1225-1236.
- Jackson, M.P.A. & Talbot, C.J. 1986. External Shapes, Strain Rates, and Dynamics of Salt Structures. *Geological Society of America Bulletin*, **97**, 305-323, [http://doi.org/10.1130/0016-7606\(1986\)97<305:Essrad>2.0.Co;2](http://doi.org/10.1130/0016-7606(1986)97<305:Essrad>2.0.Co;2).
- Jarsve, E.M., Maast, T.E., Gabrielsen, R.H., Faleide, J.I., Nystuen, J.P. & Sassier, C. 2014. Seismic stratigraphic subdivision of the Triassic succession in the Central North Sea; integrating seismic reflection and well data. *Journal of the Geological Society*, <http://doi.org/10.1144/jgs2013-056>.
- Jensen, L.N. & Schmidt, B.J. 1993. Neogene uplift and erosion offshore south Norway: magnitude and consequences for hydrocarbon exploration in the Farsund Basin. In: Spencer, A.M. (ed.) *Spec. Publ. European Association of Petroleum Geoscientists*. Springer.
- Johannessen, P.N. & Andsbjerg, J. 1993. Middle to Late Jurassic basin evolution and sandstone reservoir distribution in the Danish Central Trough. *Geological Society, London, Petroleum Geology Conference series*, **4**, 271-283, <http://doi.org/10.1144/0040271>.
- Kendall, C.G.S.C. & Schlager, W. 1981. Carbonates and relative changes in sea level. *Marine Geology*, **44**, 181-212.
- Klausen, T.G., Ryseth, A., Helland-Hansen, W. & Gjelberg, H.K. 2016. Progradational and backstepping shoreface deposits in the Ladinian to Early Norian Snadd Formation of the Barents Sea. *Sedimentology*, **63**, 893-916, <http://doi.org/10.1111/sed.12242>.
- Klausen, T.G., Ryseth, A.E., Helland-Hansen, W., Gawthorpe, R. & Laursen, I. 2015. Regional development and sequence stratigraphy of the Middle to Late Triassic Snadd Formation, Norwegian Barents Sea. *Marine and Petroleum Geology*, **62**, 102-122, <http://doi.org/10.1016/j.marpetgeo.2015.02.004>.
- Kluesner, J.W., Silver, E.A., Bangs, N.L., McIntosh, K.D., Gibson, J., Orange, D., Ranero, C.R. & von Huene, R. 2013. High density of structurally controlled, shallow to deep water fluid seep indicators imaged offshore Costa Rica. *Geochemistry, Geophysics, Geosystems*, **14**, 519-539, <http://doi.org/10.1002/ggge.20058>.
- Legler, B., Hampson, G.J., Jackson, C.A., Johnson, H.D., Massart, B.Y., Sarginson, M. & Ravnås, R. 2014. Facies relationships and stratigraphic architecture of distal, mixed tide-and wave-influenced deltaic deposits: Lower Segó sandstone, western Colorado, USA. *Journal of Sedimentary Research*, **84**, 605-625.
- Leinfelder, R.R. 1994. Distribution of Jurassic reef types: a mirror of structural and environmental changes during breakup of Pangea.
- Lewis, M.M., Jackson, C.A.L. & Gawthorpe, R.L. 2013. Salt-influenced normal fault growth and forced folding: The Stavanger Fault System, North Sea. *Journal of Structural Geology*, **54**, 156-173, <http://doi.org/10.1016/j.jsg.2013.07.015>.
- Magee, C., Duffy, O.B., Purnell, K., Bell, R.E., Jackson, C.A.L. & Reeve, M.T. 2016. Fault-controlled fluid flow inferred from hydrothermal vents imaged in 3D seismic reflection data, offshore NW Australia. *Basin Research*, **28**, 299-318, <http://doi.org/10.1111/bre.12111>.
- Mannie, A.S., Jackson, C.A.L. & Hampson, G.J. 2014. Structural controls on the stratigraphic architecture of net-transgressive shallow-marine strata in a salt-influenced rift basin: Middle-to-Upper

- Jurassic Egersund Basin, Norwegian North Sea. *Basin Research*, **26**, 675-700, <http://doi.org/10.1111/bre.12058>.
- Mannie, A.S., Jackson, C.A.-L., Hampson, G.J. & Fraser, A.J. 2016. Tectonic controls on the spatial distribution and stratigraphic architecture of a net-transgressive shallow-marine synrift succession in a salt-influenced rift basin: Middle to Upper Jurassic, Norwegian Central North Sea. *Journal of the Geological Society*, <http://doi.org/10.1144/jgs2016-033>.
- Marcon, Y., Ondréas, H., Sahling, H., Bohrmann, G. & Olu, K. 2013. Fluid flow regimes and growth of a giant pockmark. *Geology*, <http://doi.org/10.1130/g34801.1>.
- McKie, T. & Williams, B. 2009. Triassic palaeogeography and fluvial dispersal across the northwest European Basins. *Geological Journal*, **44**, 711-741, <http://doi.org/10.1002/gj.1201>.
- Michelsen, O., Nielsen, L.H., Johannessen, P.N., Andsbjerg, J. & Surlyk, F. 2003. The Jurassic of Denmark and Greenland: Jurassic lithostratigraphy and stratigraphic development onshore and offshore Denmark.
- Mogensen, T.E. & Jensen, L.N. 1994. Cretaceous subsidence and inversion along the Tornquist Zone from Kattegat to the Egersund Basin. *First Break*, **12**.
- Mogensen, T.E. & Korstgård, J.A. 2003. Triassic and Jurassic transtension along part of the Sorgenfrei-Tornquist Zone in the Danish Kattegat. *Geological Survey of Denmark and Greenland Bulletin*, **1**, 439-458.
- Montgomery, S.L. 1996. Cotton Valley lime pinnacle reef play: Branton Field. *AAPG Bulletin*, **80**, 617-629.
- Moore, C.H. 2001. *Carbonate reservoirs: porosity, evolution and diagenesis in a sequence stratigraphic framework*. Elsevier.
- Nielsen, L.H. 2003. Late Triassic–Jurassic development of the Danish Basin and the Fennoscandian Border Zone, southern Scandinavia. *The Jurassic of Denmark and Greenland. Geological Survey of Denmark and Greenland Bulletin*, **1**, 459-526.
- Olivarius, M. & Nielsen, L.H. 2016. Triassic paleogeography of the greater eastern Norwegian-Danish Basin: Constraints from provenance analysis of the Skagerrak Formation. *Marine and Petroleum Geology*, **69**, 168-182, <http://doi.org/10.1016/j.marpetgeo.2015.10.008>.
- Otvos, E.G. 2000. Beach ridges—definitions and significance. *Geomorphology*, **32**, 83-108.
- Patrino, S., Hampson, G.J. & Jackson, C.A.L. 2015a. Quantitative characterisation of deltaic and subaqueous clinofolds. *Earth-Science Reviews*, **142**, 79-119, <http://doi.org/10.1016/j.earscirev.2015.01.004>.
- Patrino, S., Hampson, G.J., Jackson, C.A.L. & Dreyer, T. 2015b. Clinofold geometry, geomorphology, facies character and stratigraphic architecture of a sand-rich subaqueous delta: Jurassic Sognefjord Formation, offshore Norway. *Sedimentology*, **62**, 350-388, <http://doi.org/10.1111/sed.12153>.
- Petersen, H., Nielsen, L., Bojesen-Koefoed, J.A., Mathiesen, A., Kristensen, L. & Dalhoff, F. 2008. Evaluation of the quality, thermal maturity and distribution of potential source rocks in the Danish part of the Norwegian–Danish Basin. *Geological Survey Of Denmark And Greenland Bulletin*, **16**.
- Phillips, T.B., Jackson, C.A.L., Bell, R.E. & Duffy, O.B. 2018. Oblique reactivation of lithosphere-scale lineaments controls rift physiography – the upper-crustal expression of the Sorgenfrei–Tornquist Zone, offshore southern Norway. *Solid Earth*, **9**, 403-429, <http://doi.org/10.5194/se-9-403-2018>.

- Phillips, T.B., Jackson, C.A.L., Bell, R.E., Duffy, O.B. & Fossen, H. 2016. Reactivation of intrabasement structures during rifting: A case study from offshore southern Norway. *Journal of Structural Geology*, **91**, 54-73, <http://doi.org/10.1016/j.jsg.2016.08.008>.
- Posamentier, H. & Laurin, P. 2005. Seismic geomorphology of oligocene to miocene carbonate buildups offshore Madura, Indonesia *SEG Technical Program Expanded Abstracts 2005*. Society of Exploration Geophysicists, 429-431.
- Prélat, A., Hodgson, D.M. & Flint, S.S. 2009. Evolution, architecture and hierarchy of distributary deep-water deposits: a high-resolution outcrop investigation from the Permian Karoo Basin, South Africa. *Sedimentology*, **56**, 2132-2154, <http://doi.org/10.1111/j.1365-3091.2009.01073.x>.
- Purkis, S., Casini, G., Hunt, D. & Colpaert, A. 2015. Morphometric patterns in Modern carbonate platforms can be applied to the ancient rock record: Similarities between Modern Alacranes Reef and Upper Palaeozoic platforms of the Barents Sea. *Sedimentary Geology*, **321**, 49-69, <http://doi.org/10.1016/j.sedgeo.2015.03.001>.
- Rattee, R.P. & Hayward, A.B. 1993. Sequence stratigraphy of a failed rift system: the Middle Jurassic to Early Cretaceous basin evolution of the Central and Northern North Sea. *Geological Society, London, Petroleum Geology Conference* 				series, **4**, 215-249, <http://doi.org/10.1144/0040215>.
- Rise, L., Bøe, R., Ottesen, D., Longva, O. & Olsen, H.A. 2008. Postglacial depositional environments and sedimentation rates in the Norwegian Channel off southern Norway. *Marine Geology*, **251**, 124-138, <http://doi.org/10.1016/j.margeo.2008.02.012>.
- Romans, B.W., Fildani, A., Hubbard, S.M., Covault, J.A., Fosdick, J.C. & Graham, S.A. 2011. Evolution of deep-water stratigraphic architecture, Magallanes Basin, Chile. *Marine and Petroleum Geology*, **28**, 612-628, <http://doi.org/10.1016/j.marpetgeo.2010.05.002>.
- Rosleff-Soerensen, B., Reuning, L., Back, S. & Kukla, P. 2012. Seismic geomorphology and growth architecture of a Miocene barrier reef, Browse Basin, NW-Australia. *Marine and Petroleum Geology*, **29**, 233-254, <http://doi.org/10.1016/j.marpetgeo.2010.11.001>.
- Ruf, A., Simo, J.A. & Hughes, T.M. 2008. Quantitative Characterization of Oligocene-Miocene Carbonate Mound Morphology from 3D Seismic Data: Applications to Geologic Modeling, East Java Basin, Indonesia. International Petroleum Technology Conference.
- Ryseth, A., Fjellbirkeland, H., Osmundsen, I.K., Skålnes, Å. & Zachariassen, E. 1998. High-resolution stratigraphy and seismic attribute mapping of a fluvial reservoir: Middle Jurassic Ness Formation, Oseberg Field. *AAPG Bulletin*, **82**, 1627-1651.
- Saller, A., Werner, K., Sugiaman, F., Cebastian, A., May, R., Glenn, D. & Barker, C. 2008. Characteristics of Pleistocene deep-water fan lobes and their application to an upper Miocene reservoir model, offshore East Kalimantan, Indonesia. *AAPG Bulletin*, **92**, 919.
- Saqab, M.M. & Bourget, J. 2016. Seismic geomorphology and evolution of early-mid Miocene isolated carbonate build-ups in the Timor Sea, North West Shelf of Australia. *Marine Geology*, **379**, 224-245, <http://doi.org/10.1016/j.margeo.2016.06.007>.
- Schlager, W. 1981. The paradox of drowned reefs and carbonate platforms. *Geological Society of America Bulletin*, **92**, 197.
- Schlager, W. 2000. Sedimentation rates and growth potential of tropical, cool-water and mud-mound carbonate systems. *Geological Society, London, Special Publications*, **178**, 217-227, <http://doi.org/10.1144/gsl.sp.2000.178.01.14>.
- Skjerven, J., Rijs, F. & Kalheim, J. 1983. Late Palaeozoic to Early Cenozoic structural development of the south-southeastern Norwegian North Sea *Petroleum Geology of the Southeastern North Sea and the Adjacent Onshore Areas*. Springer, 35-45.

- Slatt, R.M. 2006. *Stratigraphic reservoir characterization for petroleum geologists, geophysicists, and engineers*. Elsevier.
- Sneider, J.S., Clarens, P.d. & Vail, P.R. 1995. Sequence stratigraphy of the middle to upper jurassic, viking graben, north sea. *In: Steel, R.J., Felt, V.L., Johannessen, E.P. & Mathieu, C. (eds) Norwegian Petroleum Society Special Publications*. Elsevier, **5**, 167-197.
- Somme, T.O., Martinsen, O.J. & Lunt, I. 2013. Linking offshore stratigraphy to onshore paleotopography: The Late Jurassic-Paleocene evolution of the south Norwegian margin. *Geological Society of America Bulletin*, **125**, 1164-1186, <http://doi.org/10.1130/b30747.1>.
- Stewart, S. 1999. Seismic interpretation of circular geological structures. *Petroleum Geoscience*, **5**, 273-285.
- Sørensen, S. & Tangen, O.H. 1995. Exploration trends in marginal basins from Skagerrak to Stord. *In: Hanslien, S. (ed) Norwegian Petroleum Society Special Publications*. Elsevier, **Volume 4**, 97-114.
- Sørensen, S., Morizot, H. & Skottheim, S. 1992. A tectonostratigraphic analysis of the southeast Northern North Sea Basin. *In: Larsen, R.M., Brekke, H., Larsen, B.T. & Talleraas, E. (eds) Structural and Tectonic modelling and its application to Petroleum Geology*. Elsevier, Amsterdam, **1**, 19-42.
- Thybo, H. 2000. Crustal structure and tectonic evolution of the Tornquist Fan region as revealed by geophysical methods. *Bulletin of the Geological Society of Denmark*, **46**, 145-160.
- Tvedt, A.B.M., Rotevatn, A., Jackson, C.A.L., Fossen, H. & Gawthorpe, R.L. 2013. Growth of normal faults in multilayer sequences: A 3D seismic case study from the Egersund Basin, Norwegian North Sea. *Journal of Structural Geology*, **55**, 1-20, <http://doi.org/10.1016/j.jsg.2013.08.002>.
- Underhill, J.R. & Partington, M.A. 1993. Jurassic thermal doming and deflation in the North Sea: implications of the sequence stratigraphic evidence. 337-345, <http://doi.org/10.1144/0040337>.
- Vail, P.R. & Todd, R.G. 1981. Northern North Sea Jurassic unconformities, chronostratigraphy and sea-level changes from seismic stratigraphy. *Petroleum geology of the continental shelf of north-west Europe*. Heyden, London, 216-235.
- van Wees, J.D., Stephenson, R.A., Ziegler, P.A., Bayer, U., McCann, T., Dadlez, R., Gaupp, R., Narkiewicz, M., *et al.* 2000. On the origin of the Southern Permian Basin, Central Europe. *Marine and Petroleum Geology*, **17**, 43-59, [http://doi.org/10.1016/S0264-8172\(99\)00052-5](http://doi.org/10.1016/S0264-8172(99)00052-5).
- Vespremeanu-Stroe, A., Preoteasa, L., Zăinescu, F., Rotaru, S., Croitoru, L. & Timar-Gabor, A. 2016. Formation of Danube delta beach ridge plains and signatures in morphology. *Quaternary International*, **415**, 268-285, <http://doi.org/10.1016/j.quaint.2015.12.060>.
- Vollset, J. & Doré, A.G. 1984. A revised Triassic and Jurassic lithostratigraphic nomenclature for the Norwegian North Sea. *Norwegian Petroleum Directorate, Bull.*, **3**, 1-51.
- Zhang, J.-J., Wu, S.-H., Fan, T.-E., Fan, H.-J., Jiang, L., Chen, C., Wu, Q.-Y. & Lin, P. 2016. Research on the architecture of submarine-fan lobes in the Niger Delta Basin, offshore West Africa. *Journal of Palaeogeography*, **5**, 185-204, <http://doi.org/10.1016/j.jop.2016.05.005>.
- Zhuo, H., Wang, Y., Shi, H., Zhu, M., He, M., Chen, W. & Li, H. 2014. Seismic geomorphology, architecture and genesis of Miocene shelf sand ridges in the Pearl River Mouth Basin, northern South China Sea. *Marine and Petroleum Geology*, **54**, 106-122, <http://doi.org/10.1016/j.marpetgeo.2014.03.002>.
- Ziegler, P.A. 1992. North Sea Rift System. *Tectonophysics*, **208**, 55-75.